Results

We analyzed the frequency of the c.7153G>A (G2385R) substitution in 448 patients and 457 controls. Genotypes of the controls and patients were concordant with Hardy–Weinberg equilibrium. The frequency of A allele in the patients was significantly higher than in the controls ($P=1.24\times10^{-4}$, odds ratio 2.63, 95% CI 1.56–4.35, Table 2). We also detected homozygous substitution for the G2385R variant in two patients; however, we detected only the heterozygous substitution in the controls. Concerning the age at onset, the G2385R carriers were somewhat older than the noncarriers in total patients and in those <50 years of age. In contrast, the age at onset was not significantly different between carriers and noncarriers aged ≥50 years (Table 3). The disease duration was not significantly different between carriers and noncarriers (data not shown).

Discussion

In this study, we observed the *LRRK2* G2385R variant in 11.6% (52/448) of sporadic PD patients. So far, many putative pathogenic mutations have been reported including the G2385R. We detected G2385R in both patients and controls (22/457: 4.8%, Table 2); thus, this variant is not a pathogenic mutation, but a single nucleotide polymorphism. These results were similar to the allele frequencies in the Chinese [10,11]. It is estimated that mutations of *LRRK2* are the most frequent among the causative genes for autosomal dominant familial PD so far. Indeed, only one mutation (G2019S) accounted for ~6.6% of familial PD and ~1.6% of sporadic PD in Caucasians [14–16]. Interestingly, the frequency of the G2019S mutation is ~40% in the familial PD of North African Arabs [17] and ~30% in the familial PD of Ashkenazi Jews [18], whereas the G2019S mutation is a much less common mutation in Asians [19,20]. It is likely that some differences of genetic background exist among Caucasians, North African Arabs, Ashkenazi Jews, and Asians. Although G2385R has been detected only in Asian population, some risk variations in PD such as α-synuclein would be found in not only Asians but also all ethnic groups [21–24].

Among patients with age at onset <50 years, the G2385R carriers were somewhat older than noncarriers. This might indicate that G2385R has no influence on early-onset PD, and that PD of patients with early-onset might be influenced by other genetic and/or environmental factors. In addition, there were no differences in any clinical features including age at onset among carriers with homozygous or heterozygous G2385R substitution and noncarriers. Although the G2385R might increase the risk of development of PD, it does not seem to have a clear effect on modifying the symptoms or worsening the progression of the disease.

The amino-acid G2385 is located in the WD domain of LRRK2. This domain is known to bind various proteins [9]. The WD domain of LRRK2 appears to play an important role in neuronal cells. Indeed, oxidative-stress-induced cell death was more enhanced by the overexpression of G2385R variant than wild-type LRRK2 using culture cells [11]. More studies are needed to understand the functional significance of the substitution of glycine to arginine.

Conclusion

In this study, we identified that the G2385R variant in *LRRK2* is a risk for PD in Japanese population. To combine with the result of Chinese population [10,11], this variant increases the risk of PD in Asian population. So far, multiple genomic loci have been identified as susceptibility loci for PD [25], suggesting that many genes have a synergistic influence on the development of PD.

Table 1 Age characteristics of individuals

	Patients	Controls
Total sample, *n* (%)	448 (100)	457 (100)
Male, *n* (%)	217 (48.4)	240 (52.5)
Female, *n* (%)	231 (51.6)	217 (47.5)
Age at onset (years)[a]	50.7 ± 14.6 (5–89)	—
Male[a]	49.1 ± 14.8 (5–89)	—
Female[a]	52.2 ± 14.2 (7–82)	—
Age at sampling (years)[a]	59.4 ± 13.8 (15–93)	43.8 ± 16.0 (21–98)
Male[a]	57.8 ± 14.7 (15–93)	43.8 ± 14.5 (23–92)
Female[a]	60.9 ± 12.7 (22–88)	43.9 ± 17.5 (21–98)

[a]Data are mean ± SD (range).

Table 3 Comparison of age at onset of PD patients

Age at onset (years)	Carriers (*n*)	Noncarriers (*n*)	*P*-value
<50	42.5 ± 5.8 (17)	37.1 ± 9.4 (180)	0.003
≥50	59.9 ± 7.0 (33)	61.6 ± 7.8 (209)	0.24
Total	54.0 ± 10.6 (50)	50.3 ± 14.9 (389)	0.03

Data are mean ± SD.
Patients without information about age at onset (two of carriers and seven of noncarriers) were excluded from this analysis.
PD, Parkinson disease.

Table 2 Association analysis of *LRRK2* G2385R variant

	Genotype, *n* (%)			Allele, *n* (%)			
	G/G	G/A	A/A	G	A	χ^{2} [a]	*P*-value[a]
Patients (*n*=448)	396 (88.4)	50 (11.2)	2 (0.4)	842 (94.0)	54 (6.0)	14.74	1.24×10^{-4}
Controls (*n*=457)	435 (95.2)	22 (4.8)	0 (0)	892 (97.6)	22 (2.4)		

LRRK2, *Leucine-Rich Repeat kinase 2*.
[a]Compared with the control.

References

1. Polymeropoulos MH, Lavedan C, Leroy E, Ide SE, Dehejia A, Dutra A, *et al.* Mutation in the alpha-synuclein gene identified in families with Parkinson's disease. *Science* 1997; **276**:2045–2047.
2. Kitada T, Asakawa S, Hattori N, Matsumine H, Yamamura Y, Minoshima S, *et al.* Mutations in the parkin gene cause autosomal recessive juvenile parkinsonism. *Nature* 1998; **392**:605–608.
3. Leroy E, Boyer R, Auburger G, Leube B, Ulm G, Mezey E, *et al.* The ubiquitin pathway in Parkinson's disease. *Nature* 1998; **395**:451–452.
4. Bonifati V, Rizzu P, van Baren MJ, Schaap O, Breedveld GJ, Krieger E, *et al.* Mutations in the DJ-1 gene associated with autosomal recessive early-onset parkinsonism. *Science* 2003; **299**:256–259.
5. Singleton AB, Farrer M, Johnson J, Singleton A, Hague S, Kachergus J, *et al.* Alpha-synuclein locus triplication causes Parkinson's disease. *Science* 2003; **302**:841.
6. Valente EM, Abou-Sleiman PM, Caputo V, Muqit MM, Harvey K, Gispert S, *et al.* Hereditary early-onset Parkinson's disease caused by mutations in PINK1. *Science* 2004; **304**:1158–1160.
7. Paisan-Ruiz C, Jain S, Evans EW, Gilks WP, Simon J, van der Brug M, *et al.* Cloning of the gene containing mutations that cause PARK8-linked Parkinson's disease. *Neuron* 2004; **44**:595–600.
8. Zimprich A, Biskup S, Leitner P, Lichtner P, Farrer M, Lincoln S, *et al.* Mutations in LRRK2 cause autosomal-dominant parkinsonism with pleomorphic pathology. *Neuron* 2004; **44**:601–607.
9. Mata IF, Wedemeyer WJ, Farrer MJ, Taylor JP, Gallo KA. LRRK2 in Parkinson's disease: protein domains and functional insights. *Trends Neurosci* 2006; **29**:286–293.
10. Di Fonzo A, Wu-Chou YH, Lu CS, van Doeselaar M, Simons EJ, Rohe CF, *et al.* A common missense variant in the LRRK2 gene, Gly2385Arg, associated with Parkinson's disease risk in Taiwan. *Neurogenetics* 2006; **7**:133–138.
11. Tan EK, Zhao Y, Skipper L, Tan MG, Di Fonzo A, Sun L, *et al.* The LRRK2 Gly2385Arg variant is associated with Parkinson's disease: genetic and functional evidence. *Hum Genet* 2006; Sep 30 [Epub ahead of print].
12. Mata IF, Kachergus JM, Taylor JP, Lincoln S, Aasly J, Lynch T, *et al.* Lrrk2 pathogenic substitutions in Parkinson's disease. *Neurogenetics* 2005; **6**:171–177.
13. Hughes AJ, Daniel SE, Kilford L, Lees AJ. Accuracy of clinical diagnosis of idiopathic Parkinson's disease: a clinico-pathological study of 100 cases. *J Neurol Neurosurg Psychiatry* 1992; **55**:181–184.
14. Nichols WC, Pankratz N, Hernandez D, Paisan-Ruiz C, Jain S, Halter CA, *et al.* Genetic screening for a single common LRRK2 mutation in familial Parkinson's disease. *Lancet* 2005; **365**:410–412.
15. Gilks WP, Abou-Sleiman PM, Gandhi S, Jain S, Singleton A, Lees AJ, *et al.* A common LRRK2 mutation in idiopathic Parkinson's disease. *Lancet* 2005; **365**:415–416.
16. Di Fonzo A, Rohe CF, Ferreira J, Chien HF, Vacca L, Stocchi F, *et al.* A frequent LRRK2 gene mutation associated with autosomal dominant Parkinson's disease. *Lancet* 2005; **365**:412–415.
17. Lesage S, Durr A, Tazir M, Lohmann E, Leutenegger AL, Janin S, *et al.* LRRK2 G2019S as a cause of Parkinson's disease in North African Arabs. *N Engl J Med* 2006; **354**:422–423.
18. Ozelius LJ, Senthil G, Saunders-Pullman R, Ohmann E, Deligtisch A, Tagliati M, *et al.* LRRK2 G2019S as a cause of Parkinson's disease in Ashkenazi Jews. *N Engl J Med* 2006; **354**:424–425.
19. Tan EK, Shen H, Tan LC, Farrer M, Yew K, Chua E, *et al.* The G2019S LRRK2 mutation is uncommon in an Asian cohort of Parkinson's disease patients. *Neurosci Lett* 2005; **384**:327–329.
20. Tomiyama H, Li Y, Funayama M, Hasegawa K, Yoshino H, Kubo SI, *et al.* Clinicogenetic study of mutations in LRRK2 exon 41 in Parkinson's disease patients from 18 countries. *Mov Disord* 2006; **21**: 1102–1108.
21. Farrer M, Maraganore DM, Lockhart P, Singleton A, Lesnick TG, de Andrade M, *et al.* Alpha-synuclein gene haplotypes are associated with Parkinson's disease. *Hum Mol Genet* 2001; **10**: 1847–1851.
22. Pals P, Lincoln S, Manning J, Heckman M, Skipper L, Hulihan M, *et al.* Alpha-synuclein promoter confers susceptibility to Parkinson's disease. *Ann Neurol* 2004; **56**:591–595.
23. Mueller JC, Fuchs J, Hofer A, Zimprich A, Lichtner P, Illig T, *et al.* Multiple regions of alpha-synuclein are associated with Parkinson's disease. *Ann Neurol* 2005; **57**:535–541.
24. Mizuta I, Satake W, Nakabayashi Y, Ito C, Suzuki S, Momose Y, *et al.* Multiple candidate gene analysis identifies alpha-synuclein as a susceptibility gene for sporadic Parkinson's disease. *Hum Mol Genet* 2006; **15**:1151–1158.
25. Maraganore DM, de Andrade M, Lesnick TG, Strain KJ, Farrer MJ, Rocca WA, *et al.* High-resolution whole-genome association study of Parkinson disease. *Am J Hum Genet* 2005; **77**:685–693.

〔特集：蛍光ディファレンスゲル二次元電気泳動〕

蛍光ディファレンスゲル二次元電気泳動による糖尿病病態解析

山下 亮・鏑木康志

SUMMARY

Two-dimensional differential in-gel electrophoresis technology (2D DIGE) technique is highly useful for differential analysis of protein spots in two-dimensional differential gels. Utilizing this technique, we attempted to search for diabetes-related drug targets and biomarkers. In human hepatoma cell line, HepG2, we analyzed secretome in the presence or absence of a Liver X receptor agonist, TO-901317, and identified one of the up-regulated proteins in response to LXR activation as apolipoprotein E. We also evaluated nuclear proteome of cultured cells overexpressing insulin receptor substrate proteins, in which insulin-stimulated cell cycle progression is differentially regulated, and the gel pattern indicated that insulin-induced phosphorylation of a nuclear protein may be impaired in cells overexpressing cell cycle-suppressive insulin receptor substrate-3. In addition, to search for urinary markers of diabetic nephropathy using 2D DIGE, we analyzed urine samples in which most abundant proteins were removed by immunoaffinity depletion. These findings indicate that the 2D DIGE-based approach is useful for the discovery of disease-specific drug targets and diagnostic biomarkers.

Key words: secreted protein, diabetes, insulin signal, subcellular proteome, urinary proteome.

糖尿病や脂質代謝異常をはじめとする生活習慣病の急激的な増加に伴い，これらの疾患に関する研究の重要性が高まっている．現在の研究の動向としては，ゲノム情報を基に作成した網羅的アプローチ，同定された遺伝子を改変したモデル動物による疾患関連遺伝子の役割の解析，マイクロアレイを用いた遺伝子発現解析といった遺伝子を中心としたアプローチが主流となっている．ところが代謝性疾患の発症には遺伝因子のみではなく環境因子の寄与が大であり，生体内で生命現象を担うタンパク質への環境因子の影響については，分子・細胞レベルのメカニズムはほとんど未解明である．

本稿では，本研究室で蛍光ディファレンスゲル二次元電気泳動（2D DIGE）を中心としたプロテオーム解析手法を用いて行っている糖尿病やインスリン抵抗性，脂質代謝異常を対象としたいくつかのプロジェクトを以下に紹介する．

細胞由来分泌タンパク質のプロテオーム解析

脂肪組織は主なホルモン標的組織であり糖尿病の基礎研究において重要な試料となる．これまでの脂肪組織の概念として，エネルギーの貯蔵が主な役割と考えられていたが，最近ではレプチンやアディポネクチン，レジスチンといったアディポサイトカインと称される脂肪細胞から分泌され，生理活性を持つタンパク質の存在が明らかとなり，脂肪組織が内分泌器官であるという新たな概念が定着してきている．またアディポサイトカインの分泌異常は糖尿病や動脈硬化などの病態に関与しているという報告が多くなされており，これらの液性因子の疾患における意義が盛んに研究されている[1,2]．また最近では脂肪細胞[3]のみならずマクロファージ[4]や血管平滑筋[5]などから分泌されるタンパク質の網羅的解析も行われており，様々な細胞間や臓器間での分泌タンパク質を介したシグナルの伝達が示唆されている．またこのような細胞から分泌されるタンパク質

Proteomic analysis to investigate the pathogenesis of diabetes using 2D DIGE.

Ryo Yamashita, Yasushi Kaburagi; 国立国際医療センター研究所・代謝疾患研究部

Correspondence address: Yasushi Kaburagi; Department of Metabolic Disorder, Research Institute, International Medical Center of Japan, 1-21-1 Toyama, Shinjuku-ku, Tokyo 162-8655, Japan.

（受付 2006 年 6 月 20 日，受理 2006 年 6 月 30 日，刊行 2006 年 9 月 15 日）

の総体は“Secretome”と称され，プロテオーム解析やcomputational analysisによるシグナルペプチド予測などの解析から徐々に様々な細胞の分泌タンパク質が明らかになってきている．分泌タンパク質のプロテオーム解析には二次元電気泳動法や多次元クロマトグラフィー連結型タンデム質量分析法などが主に用いられている．先駆的に行われている脂肪細胞の分泌タンパク質のプロテオーム解析はいくつかのグループにより報告され，網羅的な探索と最近ではインスリンの刺激により変動する分泌タンパク質のLC-MS/MS法を用いたディファレンシャル解析も報告されている[6]．当研究室では脂肪組織と並んで主要なホルモン標的細胞である肝細胞から分泌されるタンパク質のプロテオーム解析を行っている．実験にはアルブミン合成能や糖新生などの肝特異的機能を持ち肝細胞のモデルとして汎用されているヒト肝癌由来HepG2細胞を用いた．HepG2細胞から分泌されるタンパク質のプロテオームマップはSWISS-2DPAGEで公開されているが約20種の比較的存在量が豊富なタンパク質だけで情報として乏しい[7]．われわれは，2D LC-MS/MS法によりHepG2細胞培養液中に含まれるタンパク質の網羅的な解析を行った．手法としては一般的なSecretome解析で行われるように，コンフルエント状態のHepG2細胞をphosphate-buffer saline（PBS）により数回の洗浄後に，fetal bovine serum（FBS）不含の培地にて24時間培養を行い，培地を回収した．さらに限外ろ過により濃縮・液置換した試料を解析に使用した．トリプシン消化したタンパク質試料は一次元目にイオン交換（SCX）クロマトグラフィー(Microtrap SCX, 1×8 mm 12 μm, Michrom BioResources)，二次元目に逆相（RP）クロマトグラフィー(MagicC18, 0.2×50 mm 5 μm, Michrom BioResources）を連結させた二次元HPLC（Magic 2002, Michrom BioResouces）で行った．イオン交換クロマトグラフィーはギ酸アンモニウムによる段階的な塩濃度勾配（0, 25, 50, 75, 100, 150, 250, 500 mM）による分離を行い，それぞれの溶出画分を0.1%ギ酸溶媒中に含むアセトニトリルを直線的な濃度勾配を用いた逆相クロマトグラフィーを行った．質量分析計にはエレクトロスプレーイオン源（AMR Inc.）を装備したLCQ-DECA XP Plus（Thermo Electron）を使用し，得られたMS/MSからBioworks™ソフトウェアにてタンパク質同定を行った．検索には，NCBIデータベースを用いた[8,9]．結果として89個のタンパク質が同定され，このうち分泌シグナルの有無をWebにて公開されているSignalIPにて検索を行ったところ，同定されたタンパク質の約半数はシグナルペプチドを持たないタンパク質であった．一般的なシグナルペプチドを持つ分泌タンパク質は小胞体で合成されゴルジ体に移行し細胞外に分泌されるという古典的な経路を介することが知られる．しかしながらN末端にシグナルペプチドをもたないで分泌されるタンパク質も多く存在することからその分泌過程は多岐にわたると考えられる．Volmerらも Secretome は古典的な経路と非古典的な経路などの様々な過程を介して培養液に分泌されるタンパク質を指すと，広義な定義をしている[10]．本研究からもHepG2細胞から既存の分泌タンパク質以外にも多くの存在が確認され，非古典的経路を介した分泌タンパク質の存在も示唆された．最近，核内受容体であるLXR（liver X receptor）の活性化によって肝細胞から分泌誘導され，生理活性を持つ分泌タンパク質の存在が報告されている[11]．LXRは脂肪酸中性脂肪代謝，コレステロール代謝を制御し，高脂血症や動脈硬化症などの疾患に深く関与すると考えられている．LXRの肝臓における脂質代謝の調節分子機構としては，主として肝臓において発現するLXRαアイソフォームが，RXR（retinoid X receptor）とヘテロダイマーを形成して，脂質代謝の調節関連遺伝子の転写調節を行うことが知られている．さらにLXRによって分泌誘導されるAngiopoietin like-3が血中トリグリセリドやコレステロールを調節することがわかり，肝由来の分泌タンパク質を介した脂質代謝調節機構も明らかになってきた[11]．われわれはLXRアゴニストをHepG2細胞の培養液に添加し，培養上清中のタンパク質についてディファレンシャル解析を行った（Fig. 1）．実験としてLXRアゴニスト（TO-901317）を最終濃度1 μMになるようにHepG2の培地に添加し，24時間後に回収した培養上清を限外ろ過・濃縮して試料とした．それぞれの試料を異なるCyDye（Cy3またはCy5）にてラベルし，すべての試料を混ぜたものをCy2でラベルし内部標準として，各培地間のタンパク質プロファイルの差異を2D DIGE法にて解析した．具体的には，固定化pH勾配ゲル（pH=4–7, 24 cm）を使用した一次元目等電点電気泳動後に，SDS-PAGEによる二次元目展開を行い，Typoon9400にてゲルイメージを取得後にDeCyderソフトウェア（GE Healthcare）により内部標準サンプルを介したゲル間のスポットマッチング，ディファレンシャル解析を行った．有意に変化を認めたスポットについては，ゲルをSYPRO Rubyによる染色後に再マッチングを行い，タンパク質スポットを切り出した．In-Gel Digestion法による酵素消化の後に，得られたペプチドをLC-MS/MS法にて解析した．Fig. 2に二次元電気泳動像を示す．DeCyderによる統計解析の結果，TO-901317による刺激によって，矢印で示したスポットが有意に増加変動していた．データベース検索の結果，この全てのスポットがapolipoprotein E（apoE）として同定された．さらに抗apoE抗体を用いた2-D Western blottingを行った（Fig. 3）．刺激前後の上清タンパク質を二次元電気泳動後，PVDF膜に転写し，まず全タンパク質をCy5 Mono-reactive Dye（GE Healthcare）にて染色し，続いて抗体反応を行った．抗体の検出試薬にはECL Plus（GE Healthcare）を用いた．Typoon9400（GE Healthcare）にて，それぞれの蛍光波長に

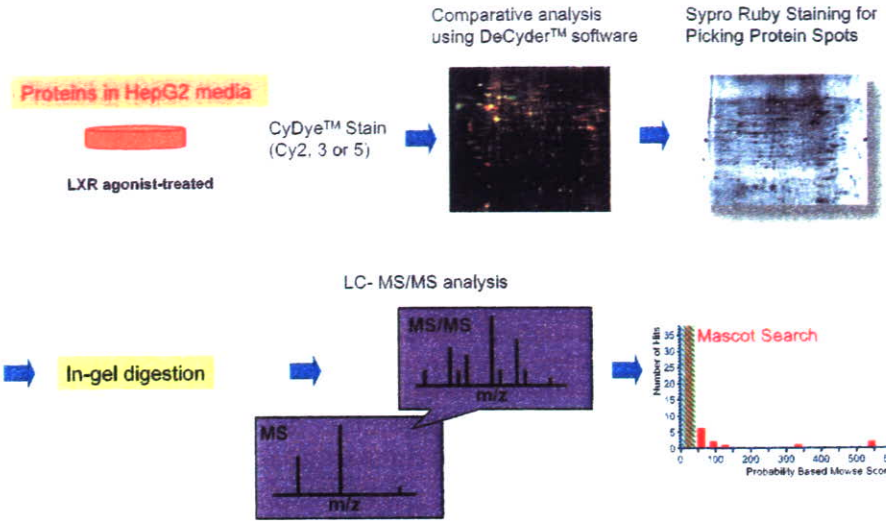

Fig. 1. Flow chart of 2D DIGE-based proteomic analysis of secreted proteins in HepG2 cells.

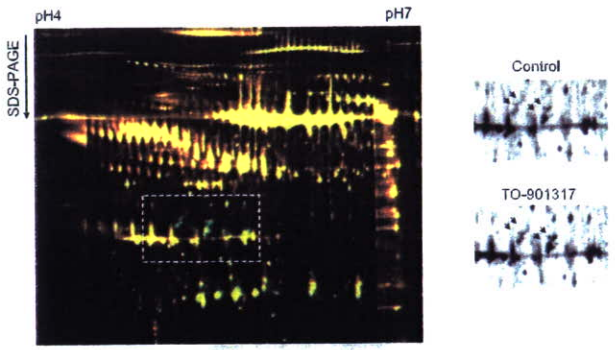

Fig. 2. 2D-DIGE analysis of secreted proteins in response to the LXR agonist T0901317 from HepG2 cells.

(A) Secreted proteins were labeled with Cy3 or Cy5, mixed, electrophoretically separated in the first dimension on pH 4–7 IPG strips and in the second dimension on a 10% polyacrylamide gel. Merge images of non-treated protein samples (red) and T0901317-treated protein samples (green). (B) Detailed 2-DE patterns of differentially expressed proteins in non-treated and T0901317-treated HepG2 cells.

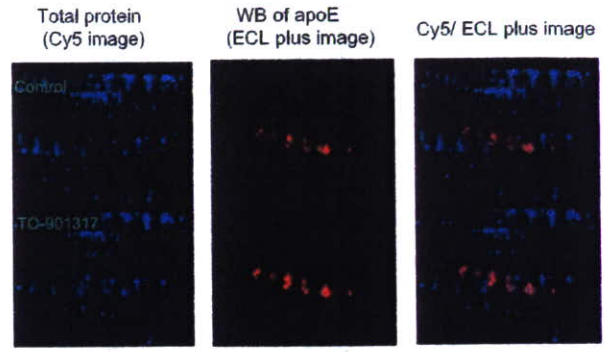

Fig. 3. Detection of T0901317-induced increase in apoE secretion by 2-D Western blotting.

Secreted proteins in response to T0901317 treatment were separated by 2-DE, transferred to a membrane, and reacted with Cy5 mono-reactive dye (Cy5 image, blue) followed by probing with anti-apoE antibodies (ECL Plus image, red).

てスキャンし，ImageQuant ソフトウェア（GE Healthcare）にて画像解析した．Cy5 Mono-reactive Dye 染色と 2D DIGE 像とは，ほぼ同様の像が得られ，また同一メンブレン上で 2 波長にてスキャンすることで，全タンパク質と抗体反応と像の正確な重ねあわせが可能となる．Fig. 3 に示すように 2-D Western blotting の結果からも LXR リガンドによって apoE の分泌が増加していることが確認された（赤色：全タンパク質，青色：apoE）．さらに apoE は幅広い pI レンジと分子量にわたって複数のスポットとして点在していることも併せて確認され，このうちの一部は糖鎖等の修飾を受けていることが推定された．apoE は LDL レセプターのリガンドのひとつであり，脂質代謝に深く関与することが知られる．これより，LXR は肝臓からのいくつかの分泌タンパク質の誘導を促し，他の臓器においても遠隔的に脂質代謝の調節を行うことが予想された．

インスリンシグナルに関与するタンパク質のプロテオーム解析

インスリンシグナル伝達機構の障害はインスリン抵抗性として知られ，2 型糖尿病をはじめとした多くの生活習慣病の発症に関与する[12]．インスリン受容体チロシンキナーゼの主要な細胞内基質である IRS（insulin receptor substrate）ファミリーは肝臓，骨格筋，脂肪組織といった古典的標的細胞をはじめとした様々な細胞において発現しており，インスリン受容体との相互作用の結果，IRS の C 末端側にある複数のチロシン残基がリン酸化される．リン酸化されたチロシン残基の多くは，様々なアダプタータンパク質と結合し，それぞれに固有の伝達経路を形成する[13]．IRS は固有のシグナル経路を介して，様々な組織特異的な生理作用を持つことが知られる．例えば肝臓においては IRS-1 と IRS-

2が重要な役割を担っており，糖新生，グリコーゲンや脂質の合成などの肝に特徴的な機能を調節していることが知られている．さらにタンパク質合成や細胞増殖，アポトーシスなど組織に共通した生理作用を持つことも知られている．またIRSアイソフォームのIRS-1，IRS-2，IRS-3各々に固有の経路や作用の存在が示唆されている[13]．これまでわれわれはIRSの糖代謝，アポトーシス抑制，細胞増殖における役割を検討しさらに，IRSの各ドメインの詳細な機能解析を行ってきた[14～17]．フローサイトメトリーによる解析にて，IRS-3高発現CHO細胞はIRS-1高発現細胞に比べてインスリン刺激によるS期への誘導が抑制され（Fig. 4A），IRS-3に特異的な細胞周期に関する経路の存在が考えられることを報告している[16]．細胞周期に関わるインスリンシグナル下流の分子について解析を行ったところ，IRS-3は他のIRSと異なって，PKB，MAPKを含む主要な経路に影響を与えずに，cyclin D1，p21，c-Myc発現低下を介して細胞周期進行を抑制することを明らかにした（Fig. 4B）．しかしながら，IRS-3に特異的な経路を規定する直接的な分

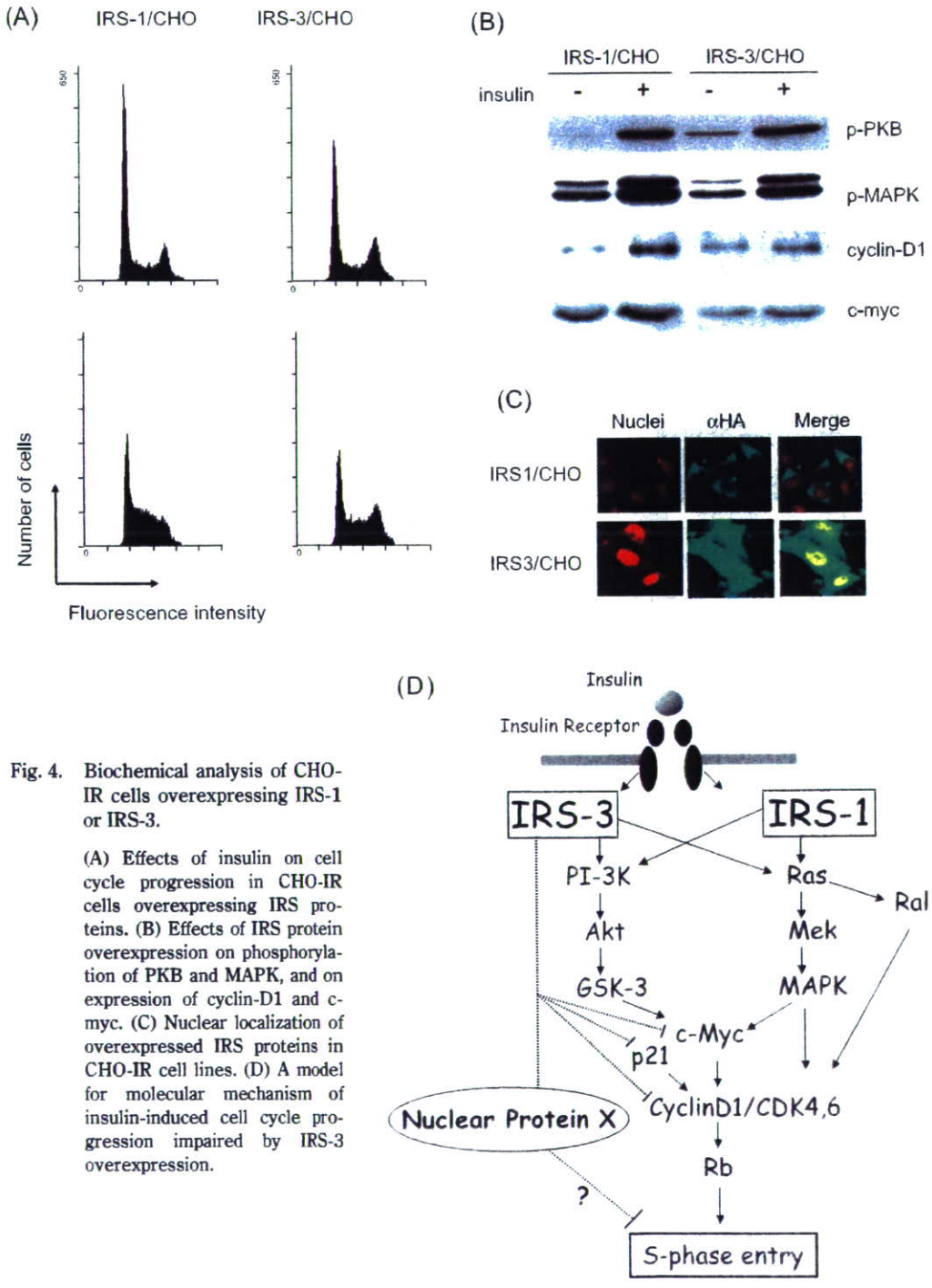

Fig. 4. Biochemical analysis of CHO-IR cells overexpressing IRS-1 or IRS-3.

(A) Effects of insulin on cell cycle progression in CHO-IR cells overexpressing IRS proteins. (B) Effects of IRS protein overexpression on phosphorylation of PKB and MAPK, and on expression of cyclin-D1 and c-myc. (C) Nuclear localization of overexpressed IRS proteins in CHO-IR cell lines. (D) A model for molecular mechanism of insulin-induced cell cycle progression impaired by IRS-3 overexpression.

子の存在が推定されるがこれまでのところわかっていない．さらにわれわれは免疫染色（Fig. 4C）にてIRS-3が核へ選択的に局在することを明らかにし，核内におけるタンパク質との相互作用などによってIRS-3特異的なシグナル経路が形成される可能性を示唆してきた（Fig. 4D）．このような標的タンパク質を検索するために，インスリンにて刺激をしたIRS-3高発現細胞のプロテオーム解析を行った．しかしながら全タンパク質を試料とした2D DIGE解析を行ったところ，IRS-3の作用に関係あるような有用な情報を得ることができなかった．最近，細胞内小器官を分画・精製しプロテオーム解析を行う，いわゆるフォーカスドプロテオミクスの手法が，より微量なタンパク質や器官に特異的なタンパク質の検出を目的として多用されてきている．また，前述したようにIRS-3は核においての機能が推測されることから，IRS-3高発現細胞の核抽出液にて2D DIGEを行うことにした．解析結果より，IRS-3高発現細胞に特異的な変動を認めるスポットが数多く見られ，その中からFig. 5に示したスポットに着目した．インスリン刺激に応じてスポットAとBが有意に変動していたが，この現象はIRS-1高発現細胞においてのみ観察され，IRS-3高発現細胞では変動がなかった．さらに3D画像からわかるように，スポットBからA，つまり酸性側にシフトする傾向があることから，このタンパク質がリン酸化されていることが推定された．LC-MS/MSによるこのスポットのタンパク質同定から，核に局在をもつタンパク質が同定された．これまでのところこのタンパク質がインスリンを含む外的な刺激でリン酸化される報告はなく，IRS-3に固有な細胞周期進行を阻害する経路に関与する可能性のあるタンパク質とみてさらなる解析を行っている．

尿タンパク質のプロテオーム解析

近年，糖尿病の増加に伴って，糖尿病性腎症に罹患する患者数が増加しており，同時に糖尿病性腎症を基礎疾患として持つ慢性透析患者の割合も多くなっている．現在，糖尿病患者における腎機能障害の最初の臨床兆候は微量アルブミン尿にて診断される．さらに糖尿病性腎症に特異性の高いIV型コラーゲンなども尿中マーカーとして用いられているが，従来のマーカーによる診断時点で腎症がすでに進行している可能性もあることから，新規の糖尿病性腎症のマーカーになりうるタンパク質やペプチドの発見が期待されている[18]．また微量アルブミン尿はさらに脳梗塞や心血管系疾患の予測因子としても知られており，他の尿中のタンパク質も疾患マーカーとして潜在的な可能性を持つと考えられる[19,20]．尿タンパク質のプロテオーム解析は二次元電気泳動法やLC-MS/MSを用いた解析により多数のグループが網羅的な同定結果を報告している．Pieperらは正常人の男女から回収した尿から分子量によりタンパク質を分画の後，二次元電気泳動を行い，MALDI-TOFとLC-MS/MSにて150種類のタンパク質を同定している[21]．またOhらも二次元電気泳動による尿プロテオームマップを作成し，113種類のタンパク質を同定している[22]．Tantipaiboonwongらは肺がんの患者の尿のプロテオーム解析を行っているが，この中で尿中のタンパク質の前処理法を検討している[23]．アセトンやTCAなどの有機溶媒を用いたタンパク質沈殿法に比して，限外ろ過膜を用いてタンパク質を濃縮し，二次元電気泳動を行うことでより多くのタンパク質スポットを検出している．最近では，Sharmaらが糖尿病性腎症の患者の尿タンパク質の2D DIGE解析を行い，alpha-1 antitrypsinが患者群において有意に尿中で高値を示すことを見出している[24]．この中で著者らは尿中のアルブミンやIgGがゲルのストリーキングを引き起こすことを問題点として提起している．

われわれの研究室では腎症をきたしていない糖尿病患者の尿のプロテオーム解析により，糖尿病性腎症への進行の臨床指標となりうる新規の早期診断マーカーや心血管系疾患などの予測マーカーの探索を目標としてプロテオーム解析を行っている．最初に尿タンパク質の2D DIGE解析応用への条件の最適化を検討した．タンパク尿をきたさない人の尿中のタンパク質は微量であり，一般的な二次元電気泳動法による解析では大量の尿が必要となる．2D DIGE法を用いる利点として，CyDyeによるタンパク質のラベルには数十μgのタンパク質があれば可能であり，少量の尿の回収で解析が可能になる．一方で，アルブミンなどの存在量の豊富なタンパク質があると多くのCyDyeがこのタンパク質のリジン残基にとられてしまうことが推定され，正確な分析を行うためにも豊富なタンパク質の除去が必要になると考えられる．このような問題を解決するため尿中の回収した尿を限界ろ過にて濃縮を行い，Albumin and IgG Removal Kit（GE Healthcare）またはMultiple Affinity Removal Spin（MARS）Cartridge（Agilent）にて高含有量タンパク質の除去を試みた．試料を再濃縮・バッファー置換を行った後に

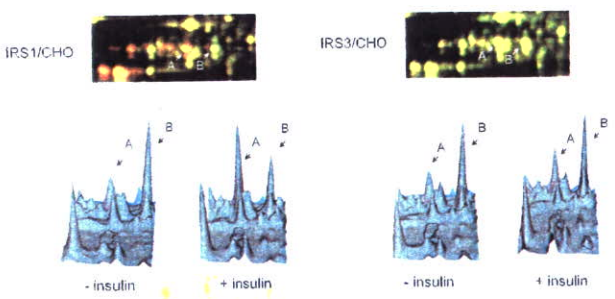

Fig. 5.　2D DIGE analysis of CHO-IR cells overexpressing IRS-1 or IRS-3 treated with insulin.

Merge images of non-treated cells (green) and insulin-treated cells (red). The 3-D views corresponding to spot A and B on 2-DE images.

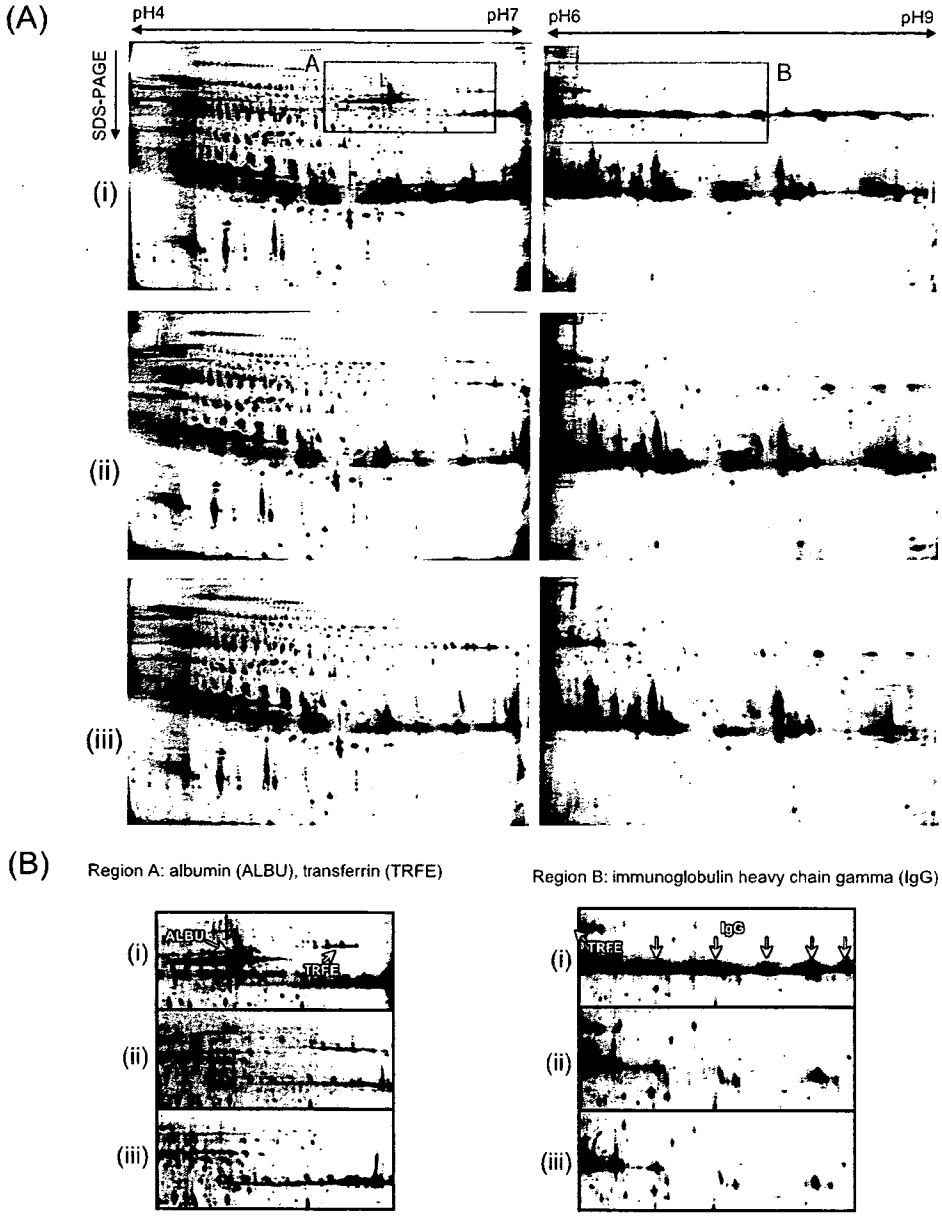

Fig. 6. 2-DE of urinary proteins after depletion of high-abundant proteins using different depletion columns.

(A) Urinary proteins were labeled with CyDye, and separated in the first dimension on pH 4–7 and 6–9 IPG strips and in the second dimension on a 10% polyacrylamide gel. (i) Crude samples; (ii) Albumin and IgG Removal Kit (GE Healthcare); (iii) MARS Cartridge (Agilent technologies). (B) Enlarged views of region A and B in 2-DE images.

CyDye にてラベルし，二次元電気泳動を行った．試験紙法にて尿タンパク陰性の尿では，ヒト血清を対象としている両者のカラム共にタンパク量の回収率は約 70% であった．Fig. 6 にカラム未使用の場合と，2 種のカラムで処理したそれぞれの泳動像を示す．タンパク質スポット数はカラム未使用と比して大きな変化はないものの Albumin と IgG のスポットは顕著に減少し，Albumin などにマスクされていたタンパク質スポットが検出可能となった．尿タンパク質を上述した方法にて処理することで，約 10 ml の尿から回収したタンパク質で二次元電気泳動が行うことができ，さらにアフィニティーカラムを用いた高含有量タンパク質の除去により，泳動のストリーキングを改善し，微量タンパク質の検出に有効であると考えられる．現在，以上の方法にて糖尿病患者尿の解析を行っている．

結　語

本研究室で行われている 2D DIGE を中心としたプロテオーム解析手法を用いた研究の一端を紹介した．本法は，同

一ゲル内で内部標準サンプルを同時に泳動することによって，サンプル間のタンパク質スポットの変動を厳密に評価することが可能であるため，糖尿病状態におけるタンパク質発現の微細な変化を検出することに適している．さらに，2D DIGE に本稿で示したような1）多次元 LC-MS/MS を用いた網羅的タンパク質同定，2）細胞小器官（オルガネラ）レベルでのプロテオーム解析，3）質量分析器での翻訳後修飾部位同定といった手法を組み合わせることによって，新規の糖尿病治療ターゲット及び診断マーカーの検索に一層の有効性を発揮するものと考える．

文　献

1) Fasshauer M, Paschke R. Regulation of adipocytokines and insulin resistance. Diabetologia 2003;46:1594–1603.
2) Kadowaki T, Yamauchi T. Adiponectin and adiponectin receptors. Endocr Rev 2005;26:439–451.
3) Kratchmarova I, Kalume DE, Blagoev B, Scherer PE, Podtelejnikov AV, Molina H, Bickel PE, Andersen JS, Fernandez MM, Bunkenborg J, Roepstorff P, Kristiansen K, Lodish HF, Mann M, Pandey A. A proteomic approach for identification of secreted proteins during the differentiation of 3T3-L1 preadipocytes to adipocytes. Mol Cell Proteomics 2002;1:213–222.
4) Dupont A, Tokarski C, Dekeyzer O, Guihot AL. Two-dimensional maps and databases of the human macrophage proteome and secretome. Proteomics 2004;4:1761–1778.
5) Dupont A, Corseaux D, Dekeyzer O, Drobecq H, Guihot AL, Susen S, Vincentelli A, Amouyel P, Jude B, Pinet F. The proteome and secretome of human arterial smooth muscle cells. Proteomics 2005;5:585–596.
6) Chen X, Cushman SW, Pannell LK, Hess S. Quantitative proteomic analysis of the secretory proteins from rat adipose cells using a 2D liquid chromatography-MS/MS approach. J Proteome Res 2005;4:570–577.
7) Sanchez JC, Appel RD, Golaz O, Pasquali C, Ravier F, Bairoch A, Hochstrasser DF. Inside SWISS-2DPAGE database. Electrophoresis 1995;16:1131–1151.
8) Yamashita R, Saito T, Satoh S, Aoki K, Kaburagi Y, Sekihara H. Effects of dehydroepiandrosterone on gluconeogenic enzymes and glucose uptake in human hepatoma cell line, HepG2. Endocr J 2005;52:727–733.
9) Yamashita R, Yasuda K, Kaburagi Y. Proteomic analysis of proteins secreted from hepatocytes. J Mass Spetrom Soc Jpn 2005;3:164–168.
10) Volmer MW, Stuhler K, Zapatka M, Schoneck A, Klein-Scory S, Schmiegel W, Meyer HE, Schwarte-Waldhoff I. Differential proteome analysis of conditioned media to detect Smad4 regulated secreted biomarkers in colon cancer. Proteomics 2005;5:2587–2601.
11) Shimamura M, Matsuda M, Kobayashi S, Ando Y, Ono M, Koishi R, Furukawa H, Makishima M, Shimomura I. Angiopoietin-like protein 3, a hepatic secretory factor, activates lipolysis in adipocytes. Biochem Biophys Res Commun 2003;301:604–609.
12) DeFronzo RA, Ferrannini E. Insulin resistance. A multifaceted syndrome responsible for NIDDM, obesity, hypertension, dyslipidemia, and atherosclerotic cardiovascular disease. Diabetes Care 1991;14:173–194.
13) White MF. IRS proteins and the common path to diabetes. Am J Physiol Endocrinol Metab 2002;283:E413–E422.
14) Kaburagi Y, Satoh S, Tamemoto H, Yamamoto-Honda R, Tobe K, Ueki K, Yamauchi T, Kono-Sugita E, Sekihara H, Aizawa S, Cushman SW, Akanuma Y, Yazaki Y, Kadowaki T. Role of insulin receptor substrate-1 and pp60 in the regulation of insulin-induced glucose transport and GLUT4 translocation in primary adipocytes. J Biol Chem 1997;272:25839–25844.
15) Kaburagi Y, Satoh S, Yamamoto-Honda R, Ito Y, Akanuma Y, Sekihara H, Yasuda K, Sasazuki T, Kadowaki T, Yazaki Y. Protection of insulin receptor substrate-3 from staurosporine-induced apoptosis. Biochem Biophys Res Commun 2003;300:371–377.
16) Kaburagi Y, Yamashita R, Ito Y, Okochi H, Yamamoto-Honda R, Yasuda K, Sekihara H, Sasazuki T, Kadowaki T, Yazaki Y. Insulin-induced cell cycle progression is impaired in chinese hamster ovary cells overexpressing insulin receptor substrate-3. Endocrinology 2004;145:5862–5874.
17) Kaburagi Y, Satoh S, Yamamoto-Honda R, Ito T, Ueki K, Akanuma Y, Sekihara H, Kimura S, Kadowaki T. Insulin-independent and wortmannin-resistant targeting of IRS-3 to the plasma membrane via its pleckstrin homology domain mediates a different interaction with the insulin receptor from that of IRS-1. Diabetologia 2001;44:992–1004.
18) Caramori ML, Fioretto P, Mauer M. The need for early predictors of diabetic nephropathy risk: is albumin excretion rate sufficient? Diabetes 2000;49:1399–1408.
19) Gerstein HC, Mann JF, Yi Q, Zinman B, Dinneen SF, Hoogwerf B, Halle JP, Young J, Rashkow A, Joyce C, Nawaz S, Yusuf S; HOPE Study Investigators. Albuminuria and risk of cardiovascular events, death, and heart failure in diabetic and nondiabetic individuals. JAMA 2001;286:421–426.
20) Hillege HL, Fidler V, Diercks GF, van Gilst WH, de Zeeuw D, van Veldhuisen DJ, Gans RO, Janssen WM, Grobbee DE, de Jong PE; Prevention of Renal and Vascular End Stage Disease (PREVEND) Study Group. Urinary albumin excretion predicts cardiovascular and noncardiovascular mortality in general population. Circulation 2002;106:1777–1782.
21) Pieper R, Gatlin CL, McGrath AM, Makusky AJ, Mondal M, Seonarain M, Field E, Schatz CR, Estock MA, Ahmed N, Anderson NG, Steiner S. Characterization of the human urinary proteome: a method for high-resolution display of urinary proteins on two-dimensional electrophoresis gels with a yield of nearly 1400 distinct protein spots. Proteomics 2004;4:1159–1174.
22) Oh J, Pyo JH, Jo EH, Hwang SI, Kang SC, Jung JH, Park EK, Kim SY, Choi JY, Lim J. Establishment of a near-standard two-dimensional human urine proteomic map. Proteomics 2004;4:3485–3497.

23) Tantipaiboonwong P, Sinchaikul S, Sriyam S, Phutrakul S, Chen ST. Different techniques for urinary protein analysis of normal and lung cancer patients. Proteomics 2005;5:1140–1149.
24) Sharma K, Lee S, Han S, Lee S, Francos B, McCue P, Wassell R, Shaw MA, RamachandraRao SP. Two-dimensional fluorescence difference gel electrophoresis analysis of the urine proteome in human diabetic nephropathy. Proteomics 2005;5:2648–2655.

Minodronate Suppresses Prostaglandin F2α-induced Vascular Endothelial Growth Factor Synthesis in Osteoblasts

Y. Hanai[1,2]
H. Tokuda[1,2]
S. Takai[1]
A. Harada[3]
T. Ohta[4]
O. Kozawa[1]

Original Basic

Abstract

In our previous study, we showed that prostaglandin $F_{2\alpha}$ ($PGF_{2\alpha}$) stimulates vascular endothelial growth factor (VEGF) synthesis via activation of p44/p42 mitogen-activated protein (MAP) kinase via protein kinase C (PKC) in osteoblast-like MC3T3-E1 cells. In addition, we demonstrated that incadronate amplified, and tiludronate suppressed $PGF_{2\alpha}$-induced VEGF synthesis among bisphosphonates, while alendronate or etidronate had no effect. In the present study, we investigated the effects of minodronate, a newly developed bisphosphonate, on $PGF_{2\alpha}$-induced VEGF synthesis in MC3T3-E1 cells. Minodronate significantly reduced VEGF synthesis induced by $PGF_{2\alpha}$ dose-dependently at levels between 3 and 100 μM. $PGF_{2\alpha}$-stimulated phosphorylation of Raf-1, MEK1/2 and p44/p42 MAP kinase were suppressed by minodronate. 12-O-tetradecanoylphorbol-13-acetate (TPA), a direct activator VEGF synthesis induced by PKC, was inhibited by minodronate. Minodronate inhibited Raf-1, MEK1/2 and p44/p42 MAP kinase phosphorylation induced by TPA. Mevalonate failed to affect the suppressive effect of minodronate on $PGF_{2\alpha}$-induced VEGF synthesis. Taken together, these results indicate that minodronate suppresses $PGF_{2\alpha}$-stimulated VEGF synthesis at the point between PKC and Raf-1 in osteoblasts.

Key Words

Bisphosphonate · prostaglandin $F_{2\alpha}$ · vascular endothelial growth factor · osteoblast

Introduction

Osteoblasts and osteoclasts are main functional cells that regulate bone metabolism. The former is responsible for bone formation, and the latter for bone resorption [1]. Bone-remodeling results from this finely coordinated process of bone resorption by activated osteoclasts coupled with subsequent deposition of new matrix by osteoblasts. Several bone-resorptive agents such as parathyroid hormone and 1,25-$(OH)_2$ vitamin D_3 upregulate RANKL (receptor activator of nuclear factor κB ligand) expression by binding specific receptors on osteoblasts, suggesting that osteoblasts also play crucial roles in the regulation of bone resorption [2]. During these processes, capillary endothelial cells along with microvasculature with osteoblasts and osteoprogenitor cells, which locally proliferate and differentiate into osteoblasts, migrate into the resorption lacuna. Therefore, osteoblasts, osteoclasts and capillary endothelial cells cooperatively regulate bone metabolism in a closely coordinated fashion via humoral factors as well as by direct cell-to-cell contact [3].

Affiliation
[1] Department of Pharmacology, Gifu University Graduate School of Medicine, Gifu, Japan
[2] Department of Clinical Laboratory, National Hospital for Geriatric Medicine, National Center for Geriatrics and Gerontology, Aichi, Japan
[3] Functional Restoration, National Hospital for Geriatric Medicine, National Center for Geriatrics and Gerontology, Aichi, Japan
[4] Internal Medicine, National Hospital for Geriatric Medicine, National Center for Geriatrics and Gerontology, Aichi, Japan

Correspondence
Osamu Kozawa · Department of Pharmacology · Gifu University Graduate School of Medicine · 1-1 Yanagido · Gifu 501-1194 · Japan · Phone: +81 (58) 230-6214 · Fax: +81 (58) 230-6215 · E-Mail: okozawa@cc.gifu-u.ac.jp

Received 12 July 2005 · **Accepted after revision** 7 December 2005

Bibliography
Horm Metab Res 2006; 38: 152–158 © Georg Thieme Verlag KG Stuttgart · New York ·
DOI 10.1055/s-2006-925177 · ISSN 0018-5043

Bisphosphonate, a stable analogue of pyrophosphate, is generally known as an inhibitor of bone resorption [4]. Bisphosphonates are widely used as a potent agent for the treatment of various metabolic bone diseases associated with increased osteoclastic bone resorption such as Paget's disease, tumoral bone disease, and osteoporosis [4]. Osteoclast recruitment, osteoclastic adhesion to bone surface and osteoclast activity inhibition is known to be the main mechanisms by which bisphosphonates inhibit bone resorptive actions [4]. In addition to osteoclasts, the inhibitory action of bisphosphonates on osteoclasts is reportedly partly mediated through its actions on osteoblasts [5,6]. In osteoblastic cell line CRP 10/30, both ibandronate and alendronate induce the synthesis of an osteoclastic bone resorption inhibitor [7]. In a previous study [8], we reported that tiludronate inhibits interleukin (IL)-6 synthesis in osteoblast-like MC3T3-E1 cells. Etidronate, alendronate, pamidronate and olpadronate prevent apoptosis of murine primary cultured osteoblasts via activation of p44/p42 mitogen-activated protein (MAP) kinase [9]. In cultured human fetal osteoblasts, pamidronate and zoledronate enhance differentiation and bone-forming activities [10]. Pamidronate and zoledronate also reportedly increase mRNA expression for osteoprotegerin in primary human osteoblasts [11]. In UMR-106-01 osteosarcoma cells, pamidronate and clodronate decrease receptor activator of nuclear factor κB ligand (RANKL) [12]. In addition, zoledronate upregulates osteocalcin and bone morphogenetic protein-2 (BMP-2) gene expression in human osteoblast-like cells [13], and decreases membrane RANKL expression by upregulating tumor necrosis factor-α-converting enzyme [14]. These studies led us to speculate that the effects of bisphosphonates on bone metabolism are not only exerted by osteoclasts, but also by osteoblasts. However, the detailed mechanism of bisphosphonate action on osteoblasts has not yet been fully clarified.

Vascular endothelial growth factor (VEGF) is a potent angiogenic factor that induces angiogenesis, endothelial cell proliferation and capillary permeability [15]. Inactivation of VEGF results in the complete suppression of vascular invasion followed by impaired trabecular bone formation and expansion of the hypertrophic chondrocyte zone in the mouse tibial epiphyseal growth plate [16]. Osteoblasts have been reported to produce and secrete VEGF in response to various physiological agonists [15,17]. In our previous studies, we reported that prostaglandin $F_{2\alpha}$ ($PGF_{2\alpha}$), a potent bone resorptive agent, activates both phosphoinositide (PI)-hydrolyzing phospholipase C (PI-phospholipase C) and phosphatidylcholine (PC)-hydrolyzing phospholipase D (PC-phospholipase D) [18,19], recognized as two major physiological protein kinase C (PKC) activation pathways [20,21], in osteoblast-like MC3T3-E1 cells. In addition, we recently showed that $PGF_{2\alpha}$ induces VEGF synthesis and secretion through PKC-dependent activation of p44/p42 MAP kinase in these cells [22]. Furthermore, we have demonstrated that incadronate enhances [22], while tiludronate suppresses [23] $PGF_{2\alpha}$-induced VEGF synthesis through activation [22] or suppression [23] of p44/p42 MAP kinase in osteoblast-like MC3T3-E1 cells, while alendronate or etidronate has little effect [22].

In the present study, we investigated the effect of minodronate, a newly developed nitrogen-containing bisphosphonate, which is structurally different and has a different side chain structure from incadronate, alendronate tiludronate or etidronate, on $PGF_{2\alpha}$-stimulated VEGF synthesis in MC3T3-E1 cells and the mechanism behind it. In contrast to the results from incadronate [22], and identical to those from tiludronate [22], this study will demonstrate that minodronate inhibits $PGF_{2\alpha}$-stimulated VEGF synthesis in these cells, and that the suppressive effect of minodronate is exerted at the point between PKC and Raf-1.

Materials and Methods

Materials

Minodronate was kindly provided by Yamanouchi Pharmaceuticals Co. Ltd. (Tokyo, Japan). $PGF_{2\alpha}$, 12-*O*-tetradecanoylphorbol-13-acetate (TPA) and mevalonate were purchased from Sigma Chemical Co. (St. Louis, MO). Phosphospecific p44/p42 MAP kinase antibodies, p44/p42 MAP kinase antibodies, phosphospecific MEK1/2 antibodies, MEK1/2 antibodies, phosphospecific Raf-1 antibodies and β-actin antibodies were purchased from New England Biolabs, Inc. (Beverly, MA). ECL Western blotting detection system was purchased from Amersham Japan (Tokyo, Japan). Mouse VEGF ELISA kit was purchased from R&D Systems, Inc. (Minneapolis, MN). Other materials and chemicals were obtained from Sigma Chemical Co. (St. Louis, MO) or Nacalai Tesque, Inc. (Kyoto, Japan). $PGF_{2\alpha}$ was dissolved in ethanol. TPA was dissolved in dimethyl sulfoxide. The maximum concentration of ethanol or dimethyl sulfoxide was 0.1%, which did not affect VEGF assay or Western blot analysis.

Cell culture

MC3T3-E1 cells are a clonal osteoblastic cell line derived from newborn mouse calvaria [24], and reportedly form mineralized matrix. In addition, we previously reported that MC3T3-E1 cells secrete osteocalcin [25] and express alkaline phosphatase [26] under our experimental conditions. MC3T3-E1 cells were maintained as previously described [27]. The cells were cultured in α-minimum essential medium (α-MEM) containing 10% fetal calf serum (FCS) at 37 °C in a humidified atmosphere of 5% CO_2/95% air. The cells were seeded into 35 mm (5×10^4) or 90 mm (2×10^5) diameter dishes in α-MEM containing 10% FCS. After five days, the medium was exchanged for α-MEM containing 0.3% FCS. The cells were used for experiments after 48 h.

Assay for VEGF

The cells were pretreated with various doses of minodronate or vehicle for 8 h, then stimulated by $PGF_{2\alpha}$ or TPA in 1 ml of α-MEM containing 0.3% FCS for the indicated period. In addition, mevalonate was added 8 h prior to stimulation by $PGF_{2\alpha}$ to investigate the involvement of mevalonate pathway on minodronate inhibition of VEGF synthesis by $PGF_{2\alpha}$. The conditioned medium was collected, and VEGF in the medium was measured by VEGF ELISA kit.

Analysis of p44/p42 MAP kinase, MEK1/2 or Raf-1

The cultured cells were pretreated with various doses of minodronate or vehicle for 8 h, then stimulated by $PGF_{2\alpha}$ or TPA in 4 ml of α-MEM containing 0.3% FCS for the indicated period. The cells were washed twice with phosphate-buffered saline and then lysed, homogenized and sonicated in a lysis buffer containing 62.5 mM Tris/HCl, pH 6.8, 2% sodium dodecyl sulfate

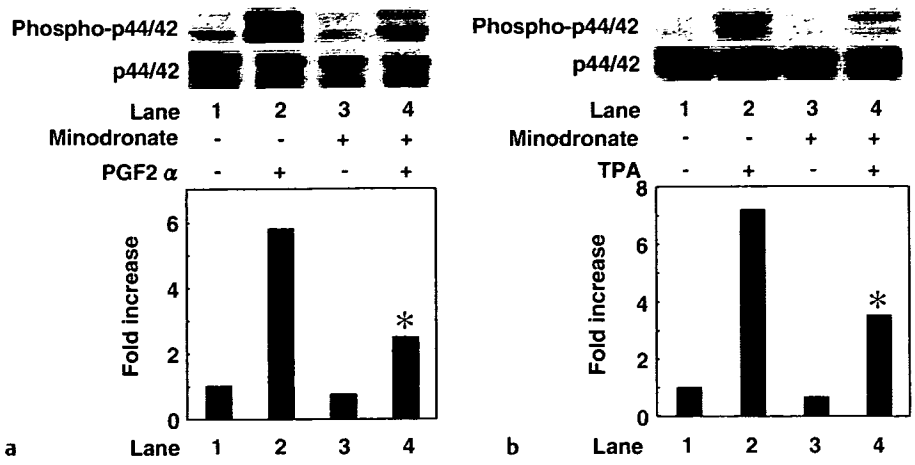

Fig. 1 Effects of minodronate on phosphorylation of p44/p42 MAP kinase induced by PGF2α or TPA in MC3T3-E1 cells. **a** Cultured cells were pretreated with 10 μM minodronate or vehicle for 8 h, then stimulated by 10 μM PGF2α or vehicle for 30 min. **b** The cultured cells were pretreated with 10 μM minodronate or vehicle for 8 h, and then stimulated by 0.1 μM TPA or vehicle for 60 min. Extracts of cells were subjected to SDS-PAGE with subsequent Western blot analysis using antibodies against phospho-specific p44/p42 MAP kinase or p44/p42 MAP kinase. The histogram shows quantitative representations of p44/p42 MAP kinase phosphorylation obtained from laser densitometric analysis. Each value represents the mean of triplicate determinations. Similar results were obtained with two additional and different cell preparations. *$p < 0.05$ compared to the value of PGF2α alone or TPA alone.

(SDS), 50 mM dithiothreitol, and 10% glycerol. SDS-PAGE was performed as described by Laemmli [28] in 10% polyacrylamide gel. Western blotting analysis was performed as described previously [29] using phosphospecific p44/p42 MAP kinase antibodies, p44/p42 MAP kinase antibodies, phosphospecific MEK1/2 antibodies, MEK1/2 antibodies, phosphospecific Raf-1 antibodies or β-actin antibodies, with peroxidase-labeled antibodies raised in goat anti-rabbit IgG used as second antibodies. Peroxidase activity on the nitrocellulose sheet was visualized on x-ray film using the ECL Western blotting detection system.

Determination of absorbance and densitometric analysis

Absorbance of ELISA samples was measured at 450 nm with a microplate spectrophotometer (Bio-Rad Laboratories, Hercules, CA). Densitometric analysis was performed using scanner and image analysis software (image J version 1.32).

Statistical analysis

Data were analyzed by ANOVA followed by Bonferroni's method for multiple comparisons between pairs, and values of $p < 0.05$ were considered significant. All data are presented as the mean ± SD from triplicate determinations. Each experiment was repeated three times with similar results.

Results

Effect of minodronate on PGF2α-induced VEGF synthesis in MC3T3-E1 cells

Recently, we have reported that $PGF_{2\alpha}$ induces VEGF synthesis in osteoblast-like MC3T3-E1 cells, and that incadronate amplifies VEGF synthesis while alendronate fails to affect synthesis [22]. Thus, we investigated the effect of minodronate on $PGF_{2\alpha}$-induced VEGF synthesis in these cells. Minodronate alone had little affect on VEGF levels, but significantly suppressed $PGF_{2\alpha}$-induced VEGF synthesis in MC3T3-E1 cells (49.1 ± 1.2 pg/ml for control; 33.1 ± 2.5pg/ml for 10μM minodronate alone, 1142.7 ± 186.5 pg/ml for 10μM $PGF_{2\alpha}$ alone; and 67.0 ± 5.5* pg/ml for 10 μM $PGF_{2\alpha}$ with 10 μM minodronate pretreatment, as measured during stimulation for 48 h; *$p < 0.05$, compared with the value of $PGF_{2\alpha}$ alone). The inhibitory effect of minodronate was dose-dependent between 3 and 100 μM (data not shown). Minodronate almost completely inhibited the $PGF_{2\alpha}$ effect at a dose of 10 μM. We confirmed that the cell number changed little by treatment [$(8.1 \pm 0.2) \times 10^5$ cells before incubation; $(7.9 \pm 0.4) \times 10^5$ cells after 48 h incubation with 100 μM minodronate; $(8.0 \pm 0.3) \times 10^5$ cells after 48 h incubation with vehicle].

Effects of minodronate on PGF2α-induced or TPA-induced phosphorylation of p44/p42 MAP kinase in MC3T3-E1 cells

In a previous study, we have demonstrated that $PGF_{2\alpha}$-induced VEGF synthesis is activated via p44/p42 MAP kinase in a PKC-dependent manner in MC3T3-E1 cells [22]. Therefore, we then investigated the detailed mechanism of minodronate underlying the inhibition of VEGF synthesis. Minodronate, which alone had little effect on phosphorylation of p44/p42 MAP kinase, markedly suppressed $PGF_{2\alpha}$-induced p44/p42 MAP kinase phosphorylation (Fig. **1 a**). According to densitometric analysis, minodronate (10 μM) caused a reduction of approximately 65% in the $PGF_{2\alpha}$ effect (*$p < 0.05$, compared with the value of $PGF_{2\alpha}$ alone).

To elucidate whether or not the effect of minodronate is exerted at a point downstream of PKC, we examined the effect of minodronate on phosphorylation of p44/p42 MAP kinase induced by TPA, a direct activator of PKC [30]. Previously, we found that p44/p42 MAP kinase was markedly phosphorylated by TPA by itself [31]. Minodronate significantly reduced p44/p42 MAP kinase phosphorylation stimulated by TPA (Fig. **1 b**). According to densitometric analysis, minodronate (10 μM) caused approximately 60% reduction in TPA effect (*$p < 0.05$, compared with the value of TPA alone).

Effect of minodronate on TPA-induced VEGF synthesis in MC3T3-E1 cells

Previously, we reported that TPA alone stimulated VEGF synthesis in osteoblast-like MC3T3-E1 cells [22]. Therefore, we investigated the effect of minodronate on TPA-induced VEGF synthesis. Minodronate significantly reduced TPA-induced syn-

Table 1 Effect of mevalonate minodronate on the TPA-induced VEGF synthesis in MC3T3-E1 cells

Minodronate	*TPA*	*VEGF (pg/ml)*
–	–	16 ± 3
–	+	280 ± 25
+	–	13 ± 2
+	+	59 ± 10*

Cultured cells were pretreated with 30 μM minodronate or vehicle for 8 h, then stimulated by 0.1 μM TPA or vehicle for 48 h. Cell viability after treatment was more than 90% of control cells. Each value represents the mean ± SD of triplicate determinations. Similar results were obtained with two additional and different cell preparations. *$p < 0.05$ compared to the value of TPA alone.

thesis of VEGF (Table 1). Minodronate (30 μM) caused a reduction of approximately 80% in TPA effect (*$p < 0.05$, compared with the value of TPA alone).

Effects of minodronate on phosphorylation of MEK1/2 induced by PGF2α or TPA in MC3T3-E1 cells

Activation of p44/p42 MAP kinase is known to be regulated by MEK1/2 as a MAP kinase kinase, which is regulated by an upstream kinase known as Raf-1 [32]. We have previously found that $PGF_{2\alpha}$ or TPA stimulates phosphorylation of both MEK1/2 and Raf-1 in osteoblast-like MC3T3-E1 cells [22]. Thus, we next examined the effect of minodronate on phosphorylation of MEK1/2 induced by $PGF_{2\alpha}$. Minodronate, which alone did not affect phosphorylation of MEK1/2, significantly suppressed $PGF_{2\alpha}$ induced MEK1/2 phosphorylation (Fig. 2a, *$p < 0.05$, compared with the value of $PGF_{2\alpha}$ alone). In addition, TPA-induced phos-

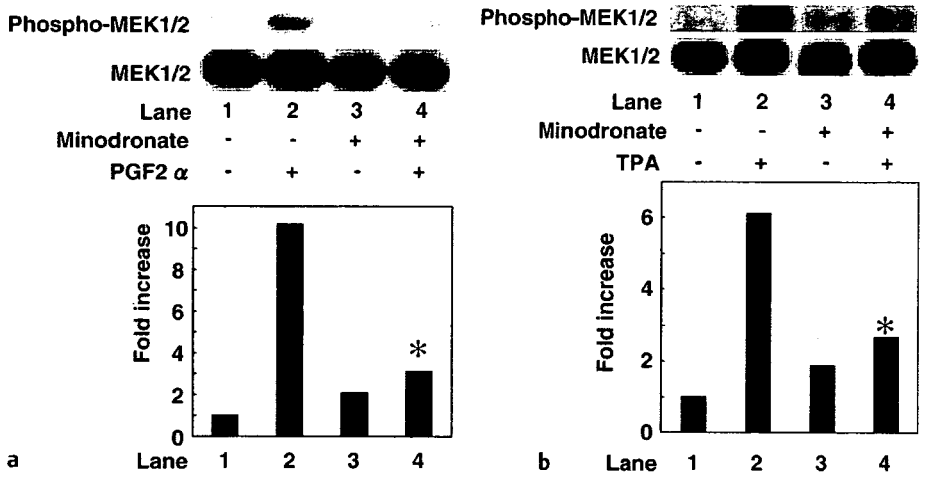

Fig. 2 Effects of minodronate on phosphorylation of MEK1/2 induced by PGF2α or TPA in MC3T3-E1 cells. (A) Cultured cells were pretreated with 10 μM minodronate or vehicle for 8 h, then stimulated by 10 μM $PGF_{2\alpha}$ or vehicle for 30 min. (B) The cultured cells were pretreated with 10 μM minodronate or vehicle for 8 h, then stimulated by 0.1 μM TPA or vehicle for 60 min. Extracts of cells were subjected to SDS-PAGE with subsequent Western blot analysis using antibodies against phosphospecific MEK1/2 or MEK1/2. The histogram shows quantitative representations of MEK1/2 phosphorylation obtained from laser densitometric analysis. Each value represents the mean of triplicate determinations. Similar results were obtained with two additional and different cell preparations. *$p < 0.05$, compared to the value of $PGF_{2\alpha}$ alone or TPA alone.

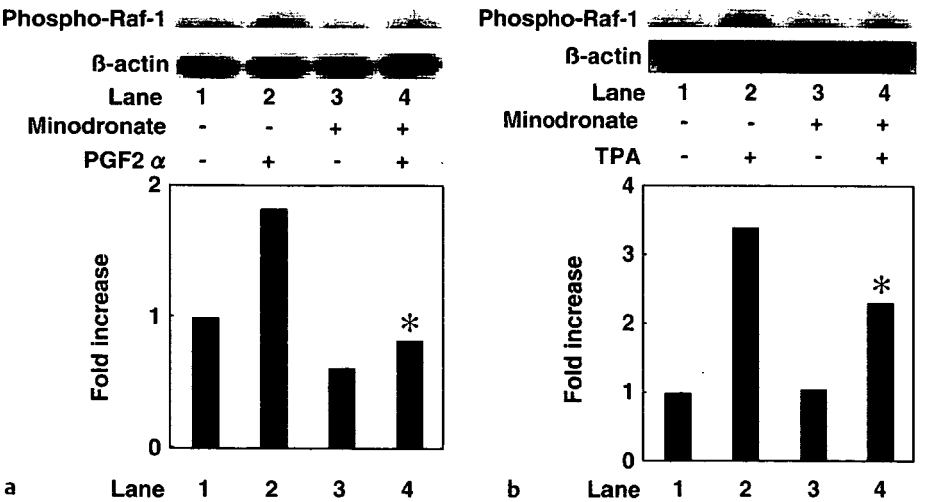

Fig. 3 Effects of minodronate on phosphorylation of Raf-1 induced by PGF2α or TPA in MC3T3-E1 cells. (**a**) The cultured cells were pretreated with 10 μM minodronate or vehicle for 8 h, then stimulated by 10 μM $PGF_{2\alpha}$ or vehicle for 15 min. (**b**) The cultured cells were pretreated with 10 μM minodronate or vehicle for 8 h, then stimulated by 0.1 μM TPA or vehicle for 60 min. Extracts of cells were subjected to SDS-PAGE with subsequent Western blot analysis using antibodies against phosphospecific Raf-1 or β-actin. The histogram shows quantitative representations of MEK1/2 phosphorylation obtained from laser densitometric analysis. Each value represents the mean of triplicate determinations. Similar results were obtained with two additional and different cell preparations. *$p < 0.05$ compared to the value of $PGF_{2\alpha}$ alone or TPA alone.

Table 2 Effect of mevalonate on minodronate inhibition of PGF2α-induced VEGF synthesis in osteoblast-like MC3T3-E1 cells

Minodronate	*Mevalonate*	*PGF2α*	*VEGF (pg/ml)*
–	–	–	33.0 ± 4.4
–	–	+	1095.0 ± 78.0
–	+	–	26.0 ± 4.5
–	+	+	1188.0 ± 282.1
+	–	–	16.0 ± 3.4
+	–	+	94.7 ± 4.2*
+	+	–	17.0 ± 3.5
+	+	+	81.3 ± 4.5*

Cultured cells were pretreated with 10 μM minodronate, 10 μM mevalonate or vehicle for 8 h, then stimulated by 10 μM $PGF_{2\alpha}$ or vehicle for 48 h. The cell viability after the treatments was more than 90% of control cells. Each value represents the mean ± SD of triplicate determinations. Similar results were obtained with two additional and different cell preparations. *$p < 0.05$, compared to the value of $PGF_{2\alpha}$ alone.

phorylation of MEK1/2 was markedly attenuated (Fig. **2b**, *$p < 0.05$, compared with the value of TPA alone).

Effects of minodronate on phosphorylation of Raf-1 induced by PGF2α or TPA in MC3T3-E1 cells

Previously, we reported that $PGF_{2\alpha}$ or TPA stimulated phosphorylation of Raf-1 in osteoblast-like MC3T3-E1 cells [22]. To clarify whether the effect of minodronate is exerted at a point upstream of Raf-1 or not, we examined the effect of minodronate on phosphorylation of Raf-1 induced by $PGF_{2\alpha}$ or TPA. Minodronate by itself did not affect Raf-1 phosphorylation, but significantly reduced phosphorylation of Raf-1 induced by $PGF_{2\alpha}$ (Fig. **3a**) or TPA (Fig. **3b**) (*$p < 0.05$, compared with the value of $PGF_{2\alpha}$ alone or TPA alone). According to densitometric analysis, minodronate (10 μM) caused a reduction of approximately 60% in the effect of $PGF_{2\alpha}$.

Effects of mevalonate on minodronate inhibition of PGF2α-induced VEGF synthesis in MC3T3-E1 cells

To clarify whether the mevalonate pathway is involved in minodronate inhibition of VEGF synthesis by $PGF_{2\alpha}$, we investigated the effect of mevalonate on the inhibition of VEGF synthesis by $PGF_{2\alpha}$ in MC3T3-E1 cells. Mevalonate, which alone had no effect on VEGF levels, did not affect either VEGF synthesis induced by $PGF_{2\alpha}$ or minodronate inhibition of $PGF_{2\alpha}$-induced VEGF synthesis (Table **2**).

Discussion

In contrast to the inhibitory effect of minodronate presented here, we have recently reported that incadronate, a nitrogen-containing bisphosphonate, but not alendronate enhances VEGF synthesis induced by $PGF_{2\alpha}$ in osteoblast-like MC3T3-E1 cells [22]. In contrast, we have recently reported that non-amino-bisphosphonate tiludronate, but not etidronate, inhibits $PGF_{2\alpha}$-induced VEGF release [23]. Thus, these findings suggest that the effects of bisphosphonates on $PGF_{2\alpha}$-induced VEGF synthesis in osteoblasts are compound-specific and vary among bisphosphonates. Pamidronate and zoledronate reportedly induce avascular necrosis of the jaw in a clinical setting [33,34], but no other bisphosphonates – including tiludronate and etidronate – are associated with avascular necrosis [33]. Taken together, the specific effects of each agent may be involved in clinical applications, supporting our present findings showing the agent-specific effects of bisphosphonates.

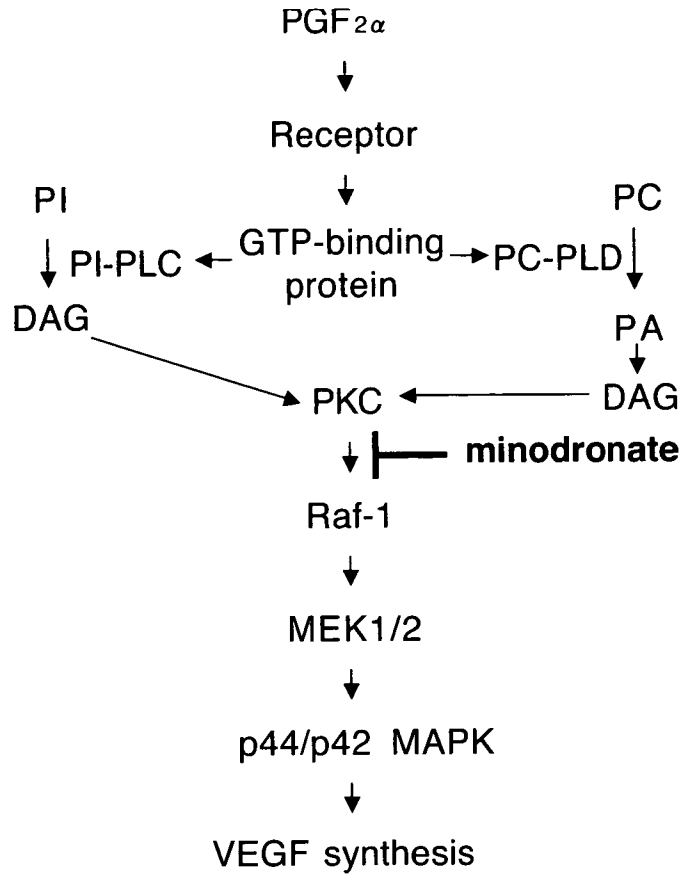

Fig. 4 Potential mechanisms in minodronate suppression of PGF2α-induced VEGF synthesis in MC3T3-E1 cells. GTP-binding protein, heterotrimeric GTP-binding protein; PI-PLC, phosphoinositide-hydrolyzing phospholipase C; PC-PLD, phosphatidylcholine-hydrolyzing phospholipase D,; PA, phosphatidic acid; DAG, diacylglycerol; PKC, protein kinase C; MAPK, mitogen-activated protein kinase; VEGF, vascular endothelial growth factor.

We previously reported that $PGF_{2\alpha}$ activated both PI-phospholipase C and PC-phospholipase D via heterotrimeric GTP-binding protein in osteoblast-like MC3T3-E1 cells [18,19], and also that $PGF_{2\alpha}$ activated p44/p42 MAP kinase in a PKC-dependent manner in these cells [35]. PI hydrolysis by phospholipase C and PC hydrolysis by phospholipase D are recognized as two major PKC-activating pathways [20,21]. In addition, we reported that $PGF_{2\alpha}$-induced VEGF synthesis through PKC-dependent, and probably PKCβI-dependent activation of p44/p42 MAP kinase in MC3T3-E1 cells [22]. Thus, we investigated the mechanism of minodronate underlying the inhibition of $PGF_{2\alpha}$-induced VEGF synthesis.

It is generally recognized that p44/p42 MAP kinase is activated through phosphorylation of threonine and tyrosine residues by dual-specificity MAP kinase kinase, known as MEK1/2 [32]. MEK1/2 is known to be activated by its own phosphorylation in-

duced by MAP kinase kinase kinase, Raf-1 [32]. We have demonstrated that minodronate also suppresses $PGF_{2\alpha}$ or TPA-induced phosphorylation of MEK1/2 and Raf-1. Taking our results as a whole, it is most likely that minodronate exerts its suppressive effect at the point between PKC and Raf-1 in $PGF_{2\alpha}$-stimulated VEGF synthesis in osteoblast-like MC3T3-E1 cells (Fig. **4**).

In the previous study, we reported that incadronate enhanced [22], while tiludronate suppressed [23] $PGF_{2\alpha}$-induced VEGF synthesis in MC3T3-E1 cells. Interestingly, the amplifying and suppressive effects of incadronate and tiludronate are exerted at a point between PKC and Raf-1 [22,23], where minodronate also showed suppressive effect in the present study. These findings suggest the different molecular mechanisms among the actions of bisphosphonates on osteoblasts, most likely their structural differences. There are considerable structural differences among these agents at the R2 side chain. Minodronate possesses 1-hydroxy-2-imidazo-(1, 2-a) pyridin-3-ylethylidene structure, and incadronate possess cycloheptylaminomethylene and 1-hydroxyethylidene structures [4], and tiludronate possesses (4-chlorophenyl) thiolmethylene structure with a more simple non-nitrogen-containing R2 side chain. In addition, the different effects of these bisphosphonates on VEGF synthesis may be related to their relative potency on anti-bone resorptive activities in these agents. In metabolic bone diseases, bone remodeling rates vary from case to case. To clarify the unique agent-specific effect(s) among bisphosphonates, it may be possible to select bisphosphonates according to the specific effect on bone-forming cells in adequate therapy by these drugs. Our present data together with our previous studies [22,23] would provide a new insight into the differences in pharmacological effects among bisphosphonates possibly due to their structural differences at the R2 side chain. Further investigation would be required to clarify the exact mechanism of bisphosphonate action on bone cells.

Nitrogen-containing bisphosphonates including minodronate are known to affect the mevalonate pathway and inhibit farnesyl diphosphate synthase [4]. We found that mevalonate did not affect the suppressive effect of minodronate on VEGF synthesis by $PGF_{2\alpha}$ in MC3T3-E1 cells. Therefore, it seems unlikely that mevalonate pathway is involved in the suppressive effect of minodronate on VEGF synthesis by $PGF_{2\alpha}$ in osteoblast-like MC3T3-E1 cells. In the present study, the effect of minodronate was significant at considerably higher doses than in clinical use. According to pharmacokinetic studies on bisphosphonates, these agents mainly accumulate in bone tissue *in vivo*[4]. Minodronate concentrations in the region probably reach much higher levels than do serum concentrations. Therefore, it is possible that the effect of minodronate shown here might be implicated in clinical relevance.

In conclusion, our present data strongly suggest that minodronate suppresses VEGF synthesis stimulated by $PGF_{2\alpha}$ in osteoblasts, and the inhibitory effect is exerted at the point between PKC and Raf-1.

Acknowledgments

This work was supported in part by a grant-in-aid for scientific research (16590873, 16591482) from the Ministry of Education, Science, Sports and Culture of Japan and research grants for longevity sciences (15A-1 and 15C-2) and health and labor sciences research grant for research on proteomics from the Ministry of Health, Labor and Welfare of Japan. The authors are very grateful to Mrs. S. Sakakibara for her skillful secretarial assistance.

References

[1] Nijweide PJ, Burger EH, Feyen JHM. Cells of bone: Proliferation, differentiation and hormonal regulation. Physiol Rev 1986; 66: 855–886

[2] Suda T, Takahashi N, Udagawa N, Jimi E, Gillespie MT, Martin TJ. Modulation of osteoclast differentiation and function by the new members of the tumor necrosis factor receptor and ligand families. Endocrine Rev 1999; 20: 345–357

[3] Erlebacher A, Filvaroff EH, Girelman SE, Derynck R. Toward a molecular understanding of skeletal development. Cell 1995; 80: 371–378

[4] Fleisch H, Reszka A, Rodan GA, Rogers M. Bisphosphonates. In: Bilezikian JP, Ratsz LG, Rodan GA (eds). Principles of Bone Biology 2nd Ed. San Diego, CA: Academic Press, 2002: 1361–1385

[5] Sahni M, Guenther HL, Fleisch H, Collin P, Martin TJ. Bisphosphonates act on rat bone resorption through the mediation of osteoblasts. J Clin Invest 1993; 91: 2004–2011

[6] Nishikawa M, Akatsu T, Katayama Y, Yasutomo Y, Kado S, Kugai N, Yamamoto M, Hagata N. Bisphosphonates act on osteoblastic cells and inhibit osteoclast formation in mouse marrow cultures. Bone 1995; 18: 9–14

[7] Vitte C, Fleisch H, Guenther HL. Bisphosphonates induce osteoblasts to secrete an inhibitor of osteoclast-mediated resorption. Endocrinology 1996; 137: 2324–2333

[8] Tokuda H, Kozawa O, Harada A, Uematsu T. Minodronate inhibits interleukin-6 synthesis in osteoblasts: Inhibition of phospholipase D activation in MC3T3-E1 cells. J Cell Biochem 1998; 69: 252–259

[9] Plotkin LI, Weinstein RS, Parfitt AM, Roberson PK, Manolagas SC, Bellido T. Prevention of osteocyte and osteoblast apoptosis by bisphosphonates and calcitonin. J Clin Invest 1999; 104: 1363–1374

[10] Reinholz GG, Getz B, Pederson L, Sanders ES, Subramaniam M, Ingle JN, Spelsberg TC. Bisphosphonates directly regulate cell proliferation, differentiation, and gene expression in human osteoblasts. Cancer Res 2000; 60: 6001–6007

[11] Viereck V, Emos G, Lauck V, Frosch KH, Blaschke S, Grundker C, Hofbauer LC. Bisphosphonates pamidronate and zoledronic acid stimulate osteoprotegerin production by primary human osteoblasts. Biochem Biophys Res Commun 2002; 291: 680–686

[12] Mackie PS, Fisher JL, Zhou H, Choong PF. Bisphosphonates regulate cell growth and gene expression in the UMR 106–01 clonal rat osteosarcoma cell line. Br J Cancer 2001; 84: 951–958

[13] Pan B, To LB, Farrugia AN, Findlay DM, Green J, Gronthos S, Evdokiou A, Lynch K, Atkins GJ, Zannettino ACW. The nitrogen-containing bisphosphonate, zoledronic acid, increases mineralization of human bone-derived cells in vitro. Bone 2004; 34: 112–123

[14] Pan B, Farrugia AN, To LB, Findlay DM, Green J, Lynch K, Zannettino ACW. The nitrogen-containing bisphosphonate, zoledronic acid, influences RANKL expression in human osteoblast-like cells by activating TNF-α converting enzyme (TACE). J Bone Miner Res 2004; 19: 147–154

[15] Ferrara N, Davis-Smyth T. The biology of vascular endothelial growth factor. Endocrine Rev 1997; 18: 4–25

[16] Gerber HP, Vu TH, Ryan AM, Kowalski J, Werb Z, Ferrara N. VEGF couples hypertrophic cartilage remodeling, ossification and angiogenesis during endochondral bone formation. Nat Med 1999; 5: 623–662

[17] Harada S, Thomas KA. Vascular endothelial growth factors. In: Bilezikian JP, Ratsz LG, Rodan GA (eds). Principles of Bone Biology 2nd Ed. San Diego, CA: Academic Press, 2002: 883–902

[18] Miwa M, Tokuda H, Tsushita K, Kotoyori J, Takahashi Y, Ozaki N, Kozawa O, Oiso Y. Involvement of pertussis toxin-sensitive GTP-binding protein in prostaglandin $F_{2\alpha}$-induced phosphoinositide hydrolysis in

osteoblast-like cells. Biochem Biophys Res Commun 1990; 171: 1229–1235
[19] Kozawa O, Suzuki A, Kotoyori J, Tokuda H, Watanabe Y, Ito Y, Oiso Y. 1994 Prostaglandin $F_{2\alpha}$ activates phospholipase D independently from activation of protein kinase C in osteoblast-like cells. J Cell Biochem 1994; 55: 373–379
[20] Nishizuka Y. Intracellular signaling by hydrolysis of phospholipids and activation of protein kinase C. Science 1992; 258: 607–614
[21] Exton JH. Regulation of phospholipase D. Biochim Biophys Acta 1999; 1439: 121–133
[22] Tokuda H, Harada A, Hirade K, Matsuno H, Ito H, Kato K, Oiso Y, Kozawa O. Incadronate amplifies prostaglandin $F_{2\alpha}$-induced vascular endothelial growth factor synthesis in osteoblasts. Enhancement of MAPK activity. J Biol Chem 2003; 278: 18930–18937
[23] Yoshida M, Tokuda H, Ishisaki A, Kanno Y, Harada A, Shimuzu K, Kozawa O. Tiludronate inhibits prostaglandin $F_{2\alpha}$-induced vascular endothelial growth factor synthesis in osteoblasts. Mol Cell Endocrinol 2005; 236: 59–66
[24] Sudo M, Kodama H, Amagai Y, Yamamoto S, Kasai S. In vitro differentiation and calcification in a new clonal osteogenic cell line derived from newborn mouse calvaria. J Cell Biol 1983; 96: 191–198
[25] Kanno Y, Ishisaki A, Yoshida M, Nakajima K, Tokuda H, Numata O, Kozawa O. Adenylyl cyclase-cAMP system inhibits thyroid hormone-stimulated osteocalcin synthesis in osteoblasts. Mol Cell Endocrinol 2005; 229: 75–82
[26] Noda T, Tokuda H, Yoshida M, Yasuda E, Hanai Y, Takai S, Kozawa O. Possible involvement of phosphatidylinositol 3-kinase/Akt pathway in insulin-like growth factor-I-induced alkaline phosphatase activity in osteoblasts. Horm Metab Res 2005; 37: 270–274
[27] Kozawa O, Suzuki A, Tokuda H, Uematsu T. Prostaglandin $F_{2\alpha}$ stimulates interleukin-6 synthesis via activation of PKC in osteoblast-like cells. Am J Physiol 1997; 272: E208–E211
[28] Laemmli UK. Cleavage of structural proteins during the assembly of the head of bacteriophage T4. Nature 1970; 227: 680–685
[29] Kato K, Ito K., Hasegawa K, Inaguma Y, Kozawa O, Asano T. Modulation of the stress-induced synthesis of hsp27 and αB-crystalin by cyclic AMP in C6 rat glioma cells. J Neurochem 1996; 66: 946–950
[30] Nishizuka Y. Studies and perspectives of protein kinase C. Science 1986; 233: 305–312
[31] Hatakeyama D, Kozawa O, Otsuka T, Shibata T, Uematsu T. Zinc suppresses IL-6 synthesis by prostaglandin F2α in osteoblasts: inhibition of phospholipase C and phospholipase D. J Cell Biochem 2002; 85: 621–628
[32] Widmann C, Gibson S, Jarpe MB, Johnson GL. Mitogen-activated protein kinase: conservation of a three-kinase module from yeast to human. Physiol Rev 1999; 79: 143–180
[33] Marx RE. Pamidronate (Aredia) and zoledronate (Zometa) induced avascular necrosis of the jaws: a growing epidemic. J Oral Maxillofac Surg 2003; 61: 1115–1118
[34] Carter GD, Goss AN. Bisphosphonates and avascular necrosis of the jaws. Aust Dent J 2003; 48: 268
[35] Tokuda H, Kozawa O, Harada A, Uematsu T. p42/p44 mitogen-activated protein kinase activation is involved in prostaglandin $F_{2\alpha}$-induced interleukin-6 synthesis in osteoblasts. Cell Signal 1999; 11: 325–330

Journal of Cellular Biochemistry 98:1249–1256 (2006)

Phosphatidylinositol 3-Kinase/Akt Plays a Role in Sphingosine 1-Phosphate-Stimulated HSP27 Induction in Osteoblasts

Shinji Takai,[1] Haruhiko Tokuda,[1,2] Rie Matsushima-Nishiwaki,[1] Yoshiteru Hanai,[1,2] Kanefusa Kato,[3] and Osamu Kozawa[1]*

[1]Department of Pharmacology, Gifu University Graduate School of Medicine, Gifu 501-1194, Japan
[2]Department of Clinical Laboratory, National Hospital for Geriatric Medicine, National Center for Geriatrics and Gerontology, Obu, Aichi 474-8511, Japan
[3]Department of Biochemistry, Institute for Developmental Research, Aichi Human Service Center, Kasugai 486-0392, Japan

Abstract We previously reported that p38 mitogen-activated protein (MAP) kinase plays a part in sphingosine 1-phosphate-stimulated heat shock protein 27 (HSP27) induction in osteoblast-like MC3T3-E1 cells. In the present study, we investigated whether phosphatidylinositol 3-kinase (PI3K)/protein kinase B (Akt) is involved in the induction of HSP27 in these cells. Sphingosine 1-phosphate time dependently induced the phosphorylation of Akt. Akt inhibitor, 1L-6-hydroxymethyl-*chiro*-inositol 2-(*R*)-2-*O*-methyl-3-*O*-octadecylcarbonate, reduced the HSP27 induction stimulated by sphingosine 1-phosphate. The sphingosine 1-phosphate-induced phosphorylation of GSK-3β was suppressed by Akt inhibitor. The sphingosine 1-phosphate-induced HSP27 levels were attenuated by LY294002 or wortmannin, PI3K inhibitors. Furthermore, LY294002 or Akt inhibitor did not affect the sphingosine 1-phosphate-induced phosphorylation of p38 MAP kinase and SB203580, a p38 MAP kinase inhibitor, had little effect on the phosphorylation of Akt. These results suggest that PI3K/Akt plays a part in the sphingosine 1-phosphate-stimulated induction of HSP27, maybe independently of p38 MAP kinase, in osteoblasts. J. Cell. Biochem. 98: 1249–1256, 2006.

Key words: sphingosine 1-phosphate; heat shock protein; protein kinase; osteoblast

Sphingosine 1-phosphate is a metabolite of sphingomyelin. It is generally recognized that sphingomyelin is catalyzed by sphingomyelinase, resulting in the formation of ceramide, which is subsequently metabolized to sphingosine and sphingosine 1-phosphate [Spiegel and Merrill, 1996]. Accumulating evidence indicates that sphingosine 1-phosphate plays an important role in essential cellular functions such as proliferation, differentiation, and migration [Spiegel and Merrill, 1996; Spiegel and Milstein, 2003; Sanchez and Hla, 2004]. Bone metabolism is regulated by two functional cells, osteoblasts and osteoclasts, responsible for bone formation and bone resorption, respectively [Nijweide et al., 1986]. As for osteoblasts, it has been reported that sphingosine 1-phosphate prevents apoptosis via phosphatidylinositol 3-kinase (PI3K) in primary calvaria rat osteoblasts and human osteosarcoma SaOS-2 cells [Grey et al., 2002]. In our study [Kozawa et al., 1997a], we have previously reported that sphingosine 1-phosphate stimulates interleukin-6 synthesis in osteoblast-like MC3T3-E1 cells. However, the exact mechanism of sphingosine 1-phosphate in bone metabolism has not yet been precisely clarified.

Heat shock proteins (HSP) are expressed in both prokaryotic and eukaryotic cells in response to the biological stress such as heat stress and chemical stress [Hendrick and Hartl, 1993]. HSPs are classified into high-molecular-weight

Grant sponsor: Ministry of Education, Science, Sports and Culture of Japan; Grant numbers: 16590873, 16591482; Grant sponsor: Ministry of Health, Labour and Welfare of Japan; Grant numbers: 15A-1, 15C-2.

*Correspondence to: Osamu Kozawa, Department of Pharmacology, Gifu University Graduate School of Medicine, Gifu 501-1194, Japan. E-mail: okozawa@cc.gifu-u.ac.jp

Received 7 November 2005; Accepted 29 December 2005
DOI 10.1002/jcb.20846
Published online 2 March 2006 in Wiley InterScience (www.interscience.wiley.com).

HSPs and low-molecular-weight HSPs based on apparent molecular sizes. Low-molecular-weight HSPs with molecular masses from 10 to 30 kDa, such as HSP27 and αB-crystallin have high homology in amino acid sequences [Inaguma et al., 1993; Benjamin and McMillan, 1998]. Though the functions of the low-molecular-weight HSPs are known less than those of the high-molecular-weight HSPs, it is generally accepted that they may have chaperoning functions like the high-molecular-weight HSPs [Inaguma et al., 1993; Benjamin and McMillan, 1998]. HSP27 becomes rapidly phosphorylated in response to various stresses, as well as to exposure to cyotokines and mitogens [Gaestel et al., 1991; Landry et al., 1992]. Under unstimulated conditions, HSP27 exists as a high-molecular weight aggregated form. It is rapidly dissociated as a result of phosphorylation [Kato et al., 1994; Rogalla et al., 1999]. The phosphorylation-induced dissociation from the aggregated form correlates with the loss of molecular chaperone activity [Kato et al., 1994; Rogalla et al., 1999]. In a previous study [Kozawa et al., 1999], we have shown that sphingosine 1-phosphate stimulates the induction of HSP27 in osteoblast-like MC3T3-E1 cells and that p38 mitogen-activated protein (MAP) kinase is involved in the HSP27 induction.

It is well known that Akt, also called protein kinase B, is a serine/threonine protein kinase that plays crucial roles in mediating intracellular signaling of variety of agonists including insulin-like growth factor-I, platelet-derived growth factor (PDGF), and cytokines [Downward, 1995; Franke et al., 1995; Coffer et al., 1998]. It has been shown that Akt regulates biological functions such as gene expression, survival, and oncogenesis [Coffer et al., 1998]. Accumulating evidence suggests that PI3K functions at an upstream from Akt [Chan et al., 1999; Cantley, 2002]. Akt containing a pleckstrin homology domain is recruited to the plasma membrane by the lipid product of PI3K and activated. As for osteoblasts, it has been reported that IGF-I and PDGF induce translocation of Akt to the nucleus [Borgatti et al., 2000]. In addition, recently, Akt is reportedly activated by cyclic stretch or androgen [Danciu et al., 2003; Kang et al., 2004]. We have recently shown that Akt plays an important role in insulin-like growth factor-I-stimulated alkaline phosphatase activity in MC3T3-E1 cells [Noda et al., 2005]. However, the correlation between HSP27 and PI3K/Akt in osteoblasts has not yet been clarified.

In the present study, we investigated whether PI3K/Akt is involved in sphingosine 1-phosphate-stimulated phosphorylation of HSP27 in osteoblast-like MC3T3-E1 cells. We here show that PI3K/Akt pathway is involved in the sphingosine 1-phosphate-stimulated induction of HSP27, maybe independently of p38 MAP kinase, in these cells.

MATERIALS AND METHODS

Materials

Sphingosine 1-phosphate and β-actin antibodies were purchased from Sigma Chemical Co. (St. Louis, MO). Akt inhibitor (1L-6-hydroxymethyl-*chiro*-inositol 2-(*R*)-2-*O*-methyl-3-*O*-octadecylcarbonate), LY294002, wortmannin, and SB203580 were obtained from Calbiochem-Novabiochem (La Jolla, CA). Phospho-specific Akt antibodies, Akt antibodies, phospho-specific p38 MAP kinase antibodies, p38 MAP kinase antibodies, phospho-specific GSK-3β antibodies, and GSK-3β antibodies were purchased from Cell Signaling Technology, Inc. (Beverly, MA). HSP27 antibodies were obtained from R&D Systems, Inc. (Minneapolis, MN). An ECL Western blotting detection system was obtained from Amersham Japan (Tokyo, Japan). Other materials and chemicals were obtained from commercial sources. Sphingosine 1-phosphate, Akt inhibitor LY294002, wortmannin, and SB203580 were dissolved in dimethyl sulfoxide (DMSO). All inhibitors became soluble in the cell culture media after once dissolved in DMSO. The maximum concentration of DMSO was 0.1%, which did not affect Western blot analysis.

Cell Culture

Cloned osteoblast-like MC3T3-E1 cells derived from newborn mouse calvaria [Sudo et al., 1983] were maintained as previously described [Kozawa et al., 1997b]. Briefly, the cells were cultured in α-minimum essential medium (α-MEM) containing 10% fetal calf serum (FCS) at 37°C in a humidified atmosphere of 5% CO_2/95% air. The cells were seeded into 90-mm diameter dishes (25×10^4/dish) in α-MEM containing 10% FCS. After 5 days, the medium was exchanged for α-MEM containing 0.3% FCS. The cells were used for experiments after 48 h. When indicated, the cells were pretreated with Akt

inhibitor, wortmannin, LY294002, or SB203580 for 60 min prior to stimulation of sphingosine 1-phosphate.

Western Blot Analysis

Cultured cells were stimulated by sphingosine 1-phosphate in serum-free α-MEM for the indicated periods. Cells were washed twice with phosphate-buffered saline and then lysed, homogenized, sonicated, and immediately boiled in a lysis buffer containing 62.5 mM Tris/Cl, pH 6.8, 2% sodium dodecyl sulfate (SDS), 50 mM dithiothreitol, and 10% glycerol. The sample was used for the analysis by Western blotting. SDS–polyacrylamide gel electrophoresis (PAGE) was performed by the method of Laemmli [Laemmli, 1970] in 10% polyacrylamide gel. Western blot analysis was performed as described previously [Kato et al., 1996], using phospho-specific Akt antibodies, Akt antibodies, HSP27 antibodies, phospho-specific p38 MAP kinase antibodies, p38 MAP kinase antibodies, phospho-specific GSK-3β antibodies, or GSK-3β antibodies with peroxidase-labeled antibodies raised in goat against rabbit IgG being used as second antibodies. Peroxidase activity on PVDF membranes was visualized on X-ray film by means of the ECL Western blotting detection system and was quantitated using NIH image software. All of Western blot analyses were repeated at least three times in independent experiments.

Statistical Analysis

The data were analyzed by ANOVA followed by Bonferroni method for multiple comparisons between pairs, and a $P<0.05$ was considered significant. All data are presented as the mean ± SD of triplicate determinations.

RESULTS

Time-Dependent Effects of Sphingosine 1-Phosphate on the Phosphorylation of Akt in MC3T3-E1 Cells

Sphingosine 1-phosphate significantly stimulates the phosphorylation of Akt in osteoblast-like MC3T3-E1 cells in a time-dependent manner (Fig. 1). The phosphorylation of Akt was markedly observed at 5 min after the sphingosine 1-phosphate-stimulation. The phosphorylation reached its peak at 15 min after the stimulation and decreased thereafter.

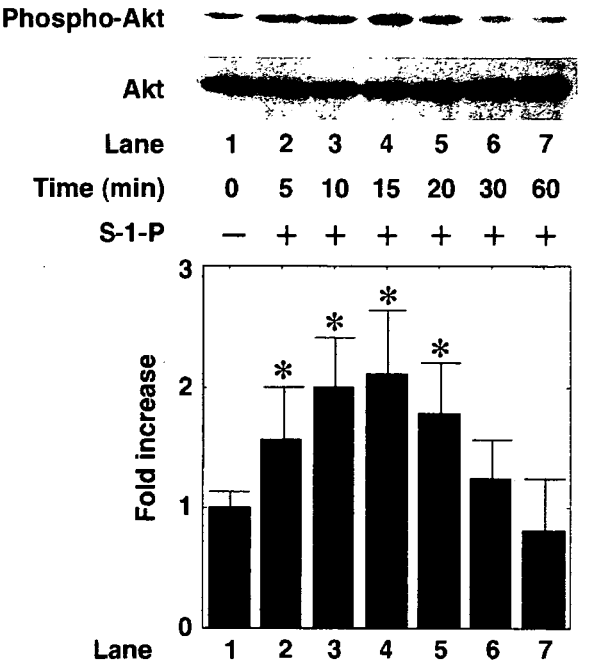

Fig. 1. Effect of sphingosine 1-phosphate (S-1-P) on the phosphorylation of Akt in MC3T3-E1 cells. The cultured cells were stimulated with 30 μM S-1-P for the indicated periods. The extracts of cells were subjected to SDS–PAGE with subsequent Western blotting analysis with antibodies against phospho-specific Akt or Akt. The histogram shows quantitative representations of the levels of S-1-P-induced phosphorylation obtained from laser densitometric analysis of three independent experiments. Similar results were obtained with two additional and different cell preparations. Each value represents the mean ± SD of triplicate determinations from triplicate independent cell preparations. *$P<0.05$, compared to the value of control.

Effect of Akt Inhibitor on the Induction of HSP27 in MC3T3-E1 Cells

Then we examined the effect of Akt inhibitor (1L-6-hydroxymethyl-*chiro*-inositol 2-(*R*)-2-*O*-methyl-3-*O*-octadecylcarbonate) [Hu et al., 2000] on the sphingosine 1-phosphate-stimulated induction of HSP27. Akt inhibitor partially suppressed the sphingosine 1-phosphate-induced up-regulation of HSP27 levels (Fig. 2). Akt inhibitor (50 μM) caused about 40% reduction in the sphingosine 1-phosphate-effect.

We have previously shown that sphingosine 1-phosphate stimulates HSP27 induction at least in part via p38 MAP kinase in osteoblasts [Kozawa et al., 1999]. However, Akt inhibitor did not influence the sphingosine 1-phosphate-induced phosphorylation of p38 MAP kinase in MC3T3-E1 cells (data not shown). It is well known that GSK-3β is one of